Notch signaling in group 3 innate lymphoid cells modulates their plasticity.

Sylvestre Chea, Thibaut Perchet, Maxime Petit, Thomas Verrier, Delphine Guy-Grand, Elena-Gaia Banchi, Christian A. J. Vosshenrich, James P Di Santo, Ana Cumano, Rachel Golub

Notch signaling in group 3 innate lymphoid cells modulates their plasticity

Sylvestre Chea,[1,2,3] Thibaut Perchet,[1,2,3] Maxime Petit,[1,2,3] Thomas Verrier,[2,3,4] Delphine Guy-Grand,[1] Elena-Gaia Banchi,[1,2,3] Christian A. J. Vosshenrich,[3,4] James P. Di Santo,[3,4] Ana Cumano,[1,2,3] Rachel Golub[1,2,3*]

[1]Institut Pasteur, Immunology Department, Lymphopoiesis Unit, 75015 Paris, France. [2]Univ. Paris Diderot, Sorbonne Paris Cité, Cellule Pasteur, 75015 Paris, France. [3]Inserm U1223, 75015 Paris, France. [4]Institut Pasteur, Immunology Department, Innate Immunity Unit, 75015 Paris, France.

[*]Corresponding author. E-mail: rachel.golub@pasteur.fr

Abstract

The Notch signaling pathway is conserved through evolution and controls processes including cell fate determination, differentiation and proliferation. It influences fate choice during hematopoiesis. Its role is well documented for the development and differentiation of lymphocytes in contrast to innate lymphoid cell (ILC) subsets. ILC are lymphoid cells without rearranged receptors that fulfill effector and regulatory functions in innate immunity and tissue remodeling. Type 3 innate lymphoid cells (ILC3s) reinforce the epithelial barrier and maintain the homeostasis with the intestinal microbiota. Here, we demonstrated that the population of natural cytotoxic receptor–positive (NCR^+) (ILC3s) in mice is composed of two subsets with distinct developmental requirements. A major subset depended on the activation of Notch2 in NCR^- ILC3 precursors in the lamina propria of the small intestine to stimulate expression of *Tbx21*, *Rorc* and *AhR*, respectively encoding T-bet, RORγt and AHR transcription factors. Notch signaling contributed to the transition of $NCR^–$ cells into NCR^+ cells in a cell-autonomous manner. In the absence of Notch signaling, $NCR^–$ ILC3s lost the gene expression profile of NCR^+ ILC3s but adopted a transcriptional profile uniquely resembling that of NCR^- ILC3s proving the absence NCR^+ precursors. A second subset of NCR^+ ILC3s did not depend on Notch for their development or for the increased expression of *Tbx21*, *Rorc*, and *AhR*; however, their production of cytokines and their cell surface abundance of the natural cytotoxic receptors were decreased. Together, our data suggest that Notch is a regulator of the plasticity of ILC3s by controlling NCR^+ cell fate.

Introduction

Innate lymphoid cells (ILCs) promote inflammatory responses and tissue homeostasis through the rapid secretion of effector cytokines at mucosal barriers and secondary lymphoid organs. These cells differentiate from a common lymphoid progenitor (CLP); however, unlike T cells or B cells, they are devoid of rearranged antigen-specific receptors. All ILCs require the transcriptional repressor Id2 for their development *(1-3)*. ILCs can be subdivided into three groups, which follow different developmental pathways and produce different cytokines (*4*). The transcriptional profiles of distinct ILC subsets in different tissues were analyzed in depth as part of the immunological genome project (*5*).

Group 1 ILCs consist of Eomes-positive conventional natural killer (cNK) cells and Eomes-negative ILC1s, secrete the inflammatory cytokine interferon-γ (IFN-γ), and require the transcription factor T-bet for proper development. ILC2s produce the cytokines interleukin-5 (IL-5) and IL-13 and are characterized by the expression of the transcription factors GATA-3 and Retinoic acid receptor related Orphan Receptor alpha (RORα). The ILC3 group is heterogeneously composed of the fetal subset of lymphoid tissue–inducer (LTi) cells (*6*) and the adult ILC3 subsets, which are mainly found at mucosal surfaces. All ILC3s depend on the transcription factor RORγt (which is encoded by *Rorc*) for their development and function, and they produce IL-17 and IL-22 (*7*). In mice, adult ILC3s can be subdivided based on the cell surface expression of the natural cytotoxic receptor 1, Natural Killer protein 46 (NKp46); mostly found present on the surface of NK cells. The $NKp46^{+}$ (NCR^{+}) subset is characterized by the cell-surface expression of the CC chemokine receptor CCR6 and produces both IL-22 and IFN-γ. The $NKp46^{-}$ (NCR^{-}) subset is composed of various sub-fractions that differently express

combinations of CD4 and CCR6 on the cell surface. Adult NKp46$^-$ CCR6$^+$ cells consist of both CD4$^+$ and CD4$^-$ cells, which share several features with LTi cells and are also called LTi-like cells. The lineage relationship between adult ILC3 subsets and the molecular mechanisms that drive their development and effector functions have been under intense investigation *(8-15)*. It was proposed that CCR6$^–$ and CCR6$^+$ ILC3s arise from distinct progenitors (*9*, *12*, *16*, *17*). Within the CCR6$^-$ population, T-bet–dependent ILC3s were identified as a source of NCR$^+$ cell precursors *(11-13)*. ILC3s exhibit plasticity in vitro and in vivo, and environmental cues, such as microbiota and IL-7, stabilize these cells by maintaining RORγt abundance (*9*). Plasticity phenomenon is recognized during T cell differentiation where the phenotypic and functional characteristics of a given population are dependent on the milieu in which they operateSeveral studies support the idea that Notch signaling is important for the generation of the NCR$^+$ ILC3 subset (*10*, *16*, *18*). It was also proposed that expression of the genes encoding T-bet and AhR by the NCR$^-$ ILC3 subset is Notch-dependent (*12*, *13*); however, the potential role of the Notch pathway in adult ILC3s has not been directly analyzed in vivo *(10-13, 19)*.

The Notch pathway is involved in several developmental processes in different tissues. Upon receptor-ligand interaction, the Notch intracellular domain (NICD) translocates into the nucleus where it acts as a transcriptional co-factor together with the recombining binding protein suppressor of hairless Kappa (RBP-Jκ). In T lymphocytes, the canonical Notch signaling pathway drives the expression of different target genes such as *Hes1*, *Tcf7* and *Dtx1*, *respectively* encoding the transcription factor HES1, TCF1 and the DTX1 protein, all important for T cell development. Notch1 is especially implicated in various stages of T cell development by

repressing B cell fate, whereas Notch2 signaling is essential for the generation of marginal zone B cells and for the development of $CD11b^+$ dendritic cells (DCs) in the spleen and intestine (*20*).

Here, we analyzed the distribution of adult ILC3 subsets in the lamina propria of mice deficient in Notch signaling through knockout of the genes encoding either Notch2 ($Il7r^{Cre/+}Notch2^{fl/fl}$ mice) or RBP-Jκ ($Il7r^{Cre/+}Rbpj^{fl/fl}$ mice) under control of the *IL7r* promoter to ensure deletion at an early stage of lymphoid cell development or of mice that exhibit enhanced Notch signaling through expression of the constitutively active Notch intracellular domain (NICD) under the control of the same promoter ($Il7r^{Cre/+}NICD$ mice). We showed that the Notch pathway was essential for the generation of NCR^+ ILC3s. Competitive bone marrow reconstitution experiments indicated that the action of the Notch pathway was direct and cell-intrinsic. Mice that exhibited constitutively active Notch signaling in the earliest lymphoid progenitors showed an increased number not only of NCR^+ cells, but also of NCR^- ILC3s, which is compatible with a role for Notch in the differentiation of NCR^+ cells from an NCR^- ILC3 subset. In contrast, mice that exhibited constitutively active Notch signaling at the later developmental $NKp46^+$ stage retained NCR^+ ILC3s that were indistinguishable from those of their littermate controls. We found that Notch acted on NCR^- precursor cells by inducing expression of the genes encoding the transcription factors T-bet, AhR, Gata3, thus enabling their differentiation into NCR^+ cells. A Notch-independent subset of NCR^+ ILC3s (around 20% of total NCR^+ ILC3s) was also identified, and these cells expressed *Tbx21* and Tcf7 independently of the Notch signaling pathway.

Results

Notch signaling regulates intestinal NCR$^+$ ILC3s

To assess roles for the Notch pathway in ILC3 homeostasis, we generated *Il7r*$^{Cre/+}$*Rbpj*$^{fl/fl}$ mice, which have defective canonical Notch signaling in all lymphoid cells because of their lack of the transcriptional co-activator RBP-Jκ. We quantified the *Rbpj* floxed alleles and determined that less than 1% of IL-7Rα$^+$ CLPs retained one *Rbpj* copy (fig. S1, A and B). In contrast, the *IL7Rα*$^{Cre/+}$ deletion in lymphoid –primed multipotent progenitors (LMPP) was restricted to a few *Rbpj* alleles. The Notch signaling pathway is essential for T cell development, which was blocked at the transitional stage between double-negative 1 (DN1) and DN2 cells (fig. S1, C and D) in *Il7r*$^{Cre/+}$*Rbpj*$^{fl/fl}$ mice; however, a few progenitors (less than 1%) escaped deletion and generated detectable peripheral T cells (fig. S1, C to F). When *Rbpj* was deleted at the hematopoietic stem cell stage in *Vav*$^{Cre/+}$*Rbpj*$^{fl/fl}$ mice, T cells were almost undetectable in the peripheral organs (fig. S1G).

We next assessed the effect of loss of Notch signaling on the composition of ILC subsets in the lamina propria of adult mice. cNK cells and ILC1s were defined by flow cytometric analysis as NK1.1$^+$NKp46$^+$IL-7Rα$^-$ and IL-7Rα$^+$ cells, respectively (Fig. 1A), whereas NCR$^+$ and NCR$^-$ ILC3s were defined as RORγt$^+$IL-7Rα$^+$NK1.1$^-$NKp46$^+$ cells and RORγt$^+$IL-7Rα$^+$NK1.1$^-$ NKp46$^-$ cells, respectively, (Fig. 1A). ILC1s and cNK cells represented less than 2% of the total number of lin$^-$ intestinal lamina propria cells, and their percentages and absolute numbers were similar in *Rbpj*-deficient and *Rbpj*-sufficient mice. We concluded that ILC1s were not affected, in terms of their total numbers or proportions, by the loss of Notch signaling (Fig. 1B).

We found that there was a 5- to 10-fold decrease in the number and percentage of NCR^+ ILC3s in *Rbpj*-deficient mice (0.8×10^4 cells, representing 1% of lamina propria lineage negative (Lin^-) cells) compared to those in *Rbpj*-sufficient or control $Il7r^{+/+}$ mice (~4×10^4 cells, representing 8%) (Fig. 1C). In contrast, the NCR^- ILC3 subset was apparently unaffected by loss of *Rbpj* (~ 9 to 10×10^4 cells, representing 15 to 20%) (Fig. 1D), which suggests that neither the development nor the maintenance of this subset required Notch signaling in vivo. The phenotypic effect of Sca1 increase and Thy1 decrease caused by the loss of Notch signaling is common to most ILC subsets with the exception of cNK cells (Fig. 1, D and E). The increase of Ly49CIFH marker, exclusively found in cNK, is compatible with the idea that NK cell precursors branch off from a common differentiation pathway before the other ILC lineages (*16, 17*). In deficient Notch signaling ILC3s, Thy1 quantities were decreased whereas only NCR^+ ILC3s showed a substantial increase in the abundance of cKit, a receptor tyrosine kinase that respond to stem cell factor for proliferation and differentiation of hematopoietic precursors (Fig. 1F). An important molecular sensor detecting "induced self" on cells in danger, the active receptor NKG2D ,was substantially less abundant in *Rbpj*-deficient cells; however, the difference in abundance was statistically significantly different only for the ILC1 and NCR^+ ILC3 subsets (Fig. 1, E and F). A comparison of the mean fluorescence intensity (MFI) of NKp46 showed that it was decreased in *Rbpj*-deficient NCR^+ ILC3s (fig. S1H). Moreover, NCR^+ ILC3s that were $NKG2D^+$ had substantially more NKp46 than did the $NKG2D^-$ subset (fig. S1I). The increased amounts of Sca1 were statistically significant in both the NCR^+ and NCR^- ILC3 subsets from the *Rbpj*-deficient mice (Fig. 1F).

We previously reported that Notch2 is found early in ILC development (*19*). In contrast to T cell development, which is mainly dependent on Notch1, ILC3 differentiation could thus be Notch2-dependent. We generated *Il7r*$^{Cre/+}$*Notch2*$^{fl/fl}$ mice and found that the number of NCR^{+} ILC3s was markedly reduced compared to those in *Il7r*$^{Cre/+}$*Notch2*$^{fl/+}$ mice (fig. S2A). Contrary to our findings with *IL7r*$^{Cre/+}$*Rbpj*$^{fl/+}$ mice, the decrease in the number of NCR^{+} ILC3s was statistically significantly different in the *IL7r*$^{Cre/+}$*Notch2*$^{fl/+}$ mice (four times less than the number of cells in *IL7r*$^{Cre/+}$*Rbpj*$^{fl/+}$ mice), suggesting that *Notch2* haplodeficiency, which results in the reduced cell-surface abundance of Notch2, was sufficient to reduce the absolute numbers of these ILCs. The absence of both *Notch2* alleles (in *IL7r*$^{Cre/+}$*Notch2*$^{f/f}$ mice) resulted in there being similar numbers of NCR^{+} and NCR^{-} cells to those found in the *IL7r*$^{Cre/+}$*Rbpj* mice. Similar to what was observed in the *IL7r*$^{Cre/+}$*Rbpj*$^{fl/fl}$ mice, no changes were found in the numbers of NCR^{-} ILC3s or in the percentages or numbers of ILC1s after *Notch2* deletion (fig. S2A).

A residual population of NCR^{+} ILC3s was still detectable in both *Il7r*$^{Cre/+}$*Notch2*$^{fl/fl}$ mice and *Il7r*$^{Cre/+}$*Rbpj*$^{fl/fl}$ mice, which might reflect incomplete Cre-mediated deletion in lymphoid progenitors. We therefore analyzed ILC3s in *Vav*$^{Cre/+}$*Rbpj*$^{fl/fl}$ mice in which peripheral T cells are undetectable, indicating complete inactivation of *Rbpj*. A small population of NCR^{+} ILC3s was also present in these mice, which is suggestive of a Notch-independent pathway for the generation of this subset (fig. S2B). Overall, the intestinal ILC subsets in *Vav*$^{Cre/+}$*Rbpj*$^{fl/fl}$ mice mirrored those found in *Il7r*$^{Cre/+}$*Rbpj*$^{fl/fl}$ mice, with reduced numbers of NCR^{+} cells, unchanged numbers of ILC1 and cNK subsets, and a small decrease in the number of NCR^{-} ILC3s (Fig. 1B and fig. S2B). An increase in the abundance of Sca1 was maintained in the ILC1 and ILC3 subsets in *Vav*$^{Cre/+}$*Rbpj*$^{fl/fl}$ mice (fig. S2C); however, an increase in the abundance of Thy1 was

observed only for the ILC1 subset (fig. S2C). Together, these results suggest that Notch signaling through Notch2 is essential for the development of appropriate numbers of NCR^+ cells, whereas a minor subset of NCR^+ ILC3s were derived through a Notch-independent pathway.

Loss of Notch signaling changes the secretive capacities of intestinal ILC3s

We next assessed whether loss of the Notch signaling pathway affected cytokine production by ILC3s and ILC1s. The abundances of mRNAs for *Il17a*, *Il17f*, *Il22*, *Csf2*, and *Ifng* were measured by quantitative RT-PCR analysis of MRNA extracted from ex vivo unstimulated sorted ILCs from the lamina propria (Fig. 2A). ILC1s did not have any T_H17 cytokine family transcripts, whereas the abundance of *Ifng* mRNA was not affected by the loss of Notch signaling. NCR^+ and NCR^- ILC3s from the $IL7r^{Cre/+}Rbpj^{fl/fl}$ mice had similar amounts of *Il22* and *Il17a* mRNAs to NCR^+ and NCR^- ILC3s from control mice (Fig. 2A). The deficiency in *Rbpj* resulted in increased amounts of C*sf2* mRNA in NCR^+ ILC3s and decreased amounts in NCR^- ILC3s, whereas *Il17f* mRNA was more abundant in the NCR^- ILC3s from $IL7r^{Cre/+}Rbpj^{fl/fl}$ mice than in the $NCR^–$ ILC3s from control mice (Fig. 2A).

Under steady-state conditions, we observed differences for *Il17f* and *Csf2* transcripts, that are both significantly increased in NCR^+ subset (Fig. 2A). IFNγ secretion was tested after Phorbol Myristate Acetate (PMA) activation, whereas the amounts of IL-17A and IL-22 proteins produced were then tested by treating intestinal ILCs with IL-23. No differences in cytokine production were observed in ILC1s from either strain of mice (Fig. 2B), whereas *Rbpj*-deficient NCR^+ ILC3s produced substantially more IL-22 than did NCR^+ ILC3s from their littermate controls. $NCR^–$ ILC3s were the major producers of IL-17A irrespective of their genotype (Fig. 2,

B and C). When we used a combination of IL-23 and PMA to activate intestinal lamina propria ILC3s (fig. S3A), we found that the NCR^- ILC3 subset of the *Rbpj*-deficient mice produced more IL-22 than did the *Rbpj*-haploinsufficient mice. The abundance of *Il1r1* mRNA was substantially decreased in NCR^- subsets compared to that in NCR^+ subsets (fig. S3B). In conclusion, these data suggest that IL-22 production from ILC3s is increased by loss of the Notch signaling pathway.

Notch signals are cell-intrinsic during the differentiation of NCR^- cells into NCR^+ ILC3s

To determine whether the decrease in the number of cells in the NCR^+ ILC3 subset of $IL7r^{Cre/+}Rbpj^{fl/fl}$ mice was a result of a direct or an indirect effect of the loss of Notch signaling, we analyzed competitively mixed bone marrow chimeric mice. The extent of reconstitution of ILCs and T cells were similar in both types of chimeras (Fig. 3). Wild-type competitor cells are more efficient to reconstitute than both $IL7r^{Cre/+}Rbpj^{fl/+}$ and $IL7r^{Cre/+}Rbpj^{fl/fl}$ donor cells since they are coming from mice deficient in one allele of *IL7Rα* (Fig. 3, A to D). This could be explained by the better proliferation and survival of both wild-type progenitor and mature cells that depend on IL-7R signaling. Hence, the reconstitution experiments were analyzed by first determining the overall percentages of the cells of interest and then by evaluating the ratio of reconstituted cells between donor cells ($CD45.1^-CD45.2^+$) and competitor cells ($CD45.1^+CD45.2^+$). Similar to what was found in the $Rbpj^{fl/fl}$ mice, intestinal ILC3 subsets in the chimeric mice were differentially affected by the loss of Notch signaling (Fig. 3, A and B). *Rbpj*-deficient or *Rbpj*-sufficient hematopoietic progenitors made similar contributions to the $CD4^+CCR6^+$ and $CD4^-CCR6^-$ cells within the NCR^- ILC3 population; however, the size of the NCR^+ ILC3 population was statistically significantly reduced among the lymphoid cells derived

from *Rbpj*-deficient progenitors as compared to that of *Rbpj*-sufficient progenitors (Fig. 3B). As expected, *Rbpj*-deficient progenitors were unable to reconstitute T cells (Fig. 3, C and D). Together, these results suggest that the mechanism for the decrease in the size of the NCR^+ population after inactivation of the Notch signaling pathway is cell-autonomous.

Intestinal NCR^+ ILC3s are derived from NCR^- precursors in a Notch signaling–dependent manner

Intestinal NCR^- ILC3s contain precursors of NCR^+ ILC3s *(11-13, 19)*. The NCR^- ILC3 subset is heterogeneous and can be subdivided based on the cell-surface expression of CD4 and CCR6. The $CCR6^+$ fraction is composed of $CD4^+$ and $CD4^-$ cells, whereas the $CCR6^-$ fraction is diverse and contains precursors that are potentially dependent on the Notch signaling pathway (*12*, *13*). We purified all three intestinal ILC3 subsets from $Il7r^{Cre/+}Rbpj^{fl/+}$ mice and $Il7r^{Cre/+}Rbpj^{fl/fl}$ mice (NCR^+, $CCR6^-NCR^-$, and $CD4^+CCR6^+NCR^-$) and analyzed the role of Notch signaling in their survival and differentiation (Fig. 4, A and B). The cell-surface abundance of IL-7Rα was reduced on a fraction of $CCR6^-$ NCR^- cells isolated from the $Il7r^{Cre/+}Rbpj^{fl/fl}$ mice (Fig. 4A). The cells were then cultured for 4 days on control OP9 stromal cells or on OP9 cells that were transduced to express the Notch ligand Delta-like 4 (OP9-Dl4 cells) (Fig. 4, C and D). The $CD4^+CCR6^+NCR^-$ ILC3 subset was stable and insensitive to Notch signaling. Substantial differences were observed in the maintenance of NCR^+ cells under both conditions. Less NCR^+ cells were maintained either in the absence of Notch ligands (that is, when cultured on OP9 cells) or in cells from $Il7r^{Cre/+}Rbpj^{fl/fl}$ mice compared to their respective controls (Fig. 4D). Conversely, we found more frequently NCR^- cells after culture of sorted NCR^+ cells on OP9 cells (Fig. 4D), which suggested a role for Notch signaling in the maintenance of NKp46, but not RORγt or IL-

7Rα, in ILCs. When CCR6$^-$NCR$^-$ cells were cultured, most of them (~60%) maintained their phenotype (Fig. 4D). Moreover, NCR$^+$ cells obtained from Notch signaling–competent precursors were 1.5 times more abundant in the presence of the Notch ligand than in its absence (Fig. 4D). The few NCR$^+$ cells that were obtained from Notch signaling–deficient precursors were insensitive to the presence of Notch ligands (Fig. 4D).

We then analyzed the abundances in the NCR$^-$ and NCR$^+$ subsets of various transcripts that are direct targets of the Notch pathway or are important for the ILC developmental program. In contrast to *Tbx21*, the genes *Dtx1, Hes1*, and *Tcf7* could be considered to be Notch-inducible during ILC development.(*21*) We found that mRNAs for these three genes were more abundant in the NCR$^-$ cells than in the NCR$^+$ cells, and were substantially decreased in the absence of Notch signaling, which suggests that the Notch pathway is active at the NCR$^-$ stage (Fig. 4E). In contrast, the abundances of *Id2*, *IL7r*, and *Gata3* mRNAs were not statistically significantly different between the NCR$^-$ and NCR$^+$ cells in the context of loss of Notch signaling (Fig. 4E and fig. S4). *Tbx21* mRNA was more abundant in NCR$^+$ cells than in the NCR$^-$ ILC3s (Fig. 4E). In both cell populations, *Tbx21* mRNA was almost undetectable in the absence of Notch signaling. We also performed intracellular staining of ILC1s, NCR$^-$ cells, and NCR$^+$ cells (Fig. 4F). Whereas T-bet was similarly low in abundance in all ILC3 subsets, confirming its essential role in the generation of NCR$^+$ cells, RORγt protein was substantially reduced in cells from the *Il7r*$^{Cre/+}$*Rbpj*$^{fl/fl}$ mice (Fig. 4G). These results suggest that two distinct pools of NCR$^+$ ILC3s differentiate in the lamina propria through *Rbpj*-dependent and *Rbpj*-independent pathways, and that the Notch signaling pathway operates in NCR$^-$ ILC3s by increasing not only the abundance of RORγt, but also the expression of *Tcf7* and *Tbx21*.

Notch signaling directly stimulates the development of NCR$^-$ ILC3 precursors into NCR$^+$ ILC3s

To complement our analyses of the role of the Notch signaling pathway on ILC3s, we generated mice with constitutive expression of the Notch intracellular domain (NICD) in lymphoid cells (*Il7r*$^{Cre/+}$*NICD* mice) (Fig. 5A). The percentages and total numbers of CCR6$^-$NCR$^-$ cells and NCR$^+$ ILC3s were statistically significantly increased in *Il7r*$^{Cre/+}$*NICD* mice compared to those in the control mice, whereas the number of CCR6$^+$NCR$^-$ ILC3s remained unchanged (Fig. 5B). These results indicated that the Notch pathway was active in the CCR6$^-$ NCR$^-$ cells. There was no increase in the mRNAs of pro-apoptotic genes in the absence of Notch signaling (fig. S5). Thus, we concluded that the absence of a large fraction of NCR$^+$ ILC3s in Notch signaling–deficient mice was not a result of increased apoptosis, but rather to a low rate of differentiation. We did not detect the decreased expression of any gene encoding pro-survival factors in the absence of Notch signaling (fig. S5). On the contrary, the only difference detected in the absence of Notch signaling was the increase of the pro-survival gene Bcl2 in NCR$^-$ precursors (fig. S5). Hence, the increased numbers of ILC3s in the *IL-7rα*^{Cre}*-Rosa26*$^{NICD/+}$ mice with a constitutive activation of the Notch signaling pathway was likely not because of the increased survival of these cells.

We further tested whether Notch signaling also affected developing NCR$^+$ ILC3s by analyzing ILCs in the lamina propria of *Ncr1*$^{Cre/+}$*NICD* mice, that constitutively express the active form of Notch in all cells expressing Ncr1 (Nkp46). We found that all three ILC3 subsets were unchanged in percentages and numbers (Fig. 5, C and D). All subsets of ILC3s also had similar

amounts of RORγt, NKp46, and IL-7Rα (fig. S6A). We concluded that the Notch signaling pathway had no effect on the survival of NCR^+ ILC3s. The MFI of NKp46 was increased in NCR^+ ILC3s expressing NICD, which is consistent with a role for Notch signaling in regulating the cell-surface abundance of NKp46 (Fig. 5E), whereas the abundance of RORγt was unchanged in all ILC3 subsets (Fig. 5F). Furthermore, the total number of intestinal ILC1s was increased in the NICD-expressing mice (Fig. 5G). Because NICD had no effect on the ratio of NCR^+ ILC3s among total ILCs or the abundance of RORγt, we propose that constitutive activation of the Notch signaling pathway at the NKp46-positive stage increased the size of the ILC1 and cNK subsets independently of a potential ILC3-ILC1 plasticity. Moreover, flow cytometric analysis of the cell surface amounts of both IL-7Rα and Dx5 enabled the identification of ILC1s among total $NKp46^+NK1.1^+$ cells, and tended to show that percentage of ILC1s was decreased among group 1 ILCs (fig. S6B). Together, these results support our conclusion that Notch has a direct role on the differentiation of NCR^- precursors into NCR^+ cells in the intestine, rather than modulating the survival or plasticity of $NKp46^+$ ILC3s.

In the absence of Notch signaling, the population of $CCR6^-NCR^-$ cells is devoid of Notch-dependent precursors of NCR^+ cells

We hypothesized that the maturation of NCR^- ILC3 precursors into NCR^+ ILC3s is blocked in the absence of canonical Notch signaling. Thus, we investigated the effect of loss of the Notch signaling pathway on the transcriptional profiles of different NCR^- ILC3 subsets. All NCR^- ILC3 subsets ($CD4^+CCR6^+$, $CD4^-CCR6^+$, and $CD4^-CCR6^-$) were present at comparable percentages and numbers in the lamina propria of *Rbpj*-deficient and *Rbpj*-haploinsufficient mice (Fig. 6, A and B). We then analyzed the transcriptional profiles, in Notch signaling–competent

and –deficient cells, of a set of transcripts that includes transcription factors, chemokines, and cytokine receptors expressed in ILCs, as well as components of the Notch signaling pathway. We also analyzed ILC1s, $CD4^+CCR6^+$ ILC3s, and $CD4^-CCR6^+$ ILC3s and compared them to the NCR^+ and $CCR6^-NCR^-$ ILC3 subsets. Genes with low expression overall [less than 20-fold of that of *Tbp* (<3 mRNA molecules per cell) (*22*)] were removed from the analysis, and the abundances of all mRNAs were normalized to the average mRNA abundances of the housekeeping genes *Actb*, *Gapdh*, and *Hprt*.

Clustering of the samples and transcripts enabled the definition of gene signatures that characterized each subpopulation (Fig. 6C). ILC1s were separated from ILC3 subsets, whereas $CD4^+CCR6^+$ ILC3s clustered together with $CD4^-CCR6^+$ ILC3s, confirming their close relationship. Only for $CCR6^-NCR^-$ ILCs did cells from $Il7r^{Cre/+}Rbpj^{fl/fl}$ mice not cluster with cells from $Il7r^{Cre/+}Rbpj^{fl/+}$ mice, consistent with their dependence on Notch signaling. $CCR6^-NCR^-$ cells from $Il7r^{Cre/+}Rbpj^{fl/+}$ mice clustered with NCR^+ ILC3s, whereas cells from $Il7r^{Cre/+}Rbpj^{fl/fl}$ mice clustered with other NCR^- ILC3 subsets. Target genes were identified as either decreased in expression (Fig. 6D, top) or increased in expression (Fig. 6D, bottom) with at least a 1.5-fold change in NCR^+ cells, $CCR6^-NCR^-$ ILC3s, and $CCR6^+NCR^-$ ILC3s from $Il7r^{Cre/+}Rbpj^{fl/fl}$ mice compared to haploinsufficient mice. .$CCR6^-NCR^-$ ILC3s were the cells that showed the largest number of genes that were decreased in expression (20 genes) compared to those in $CCR6^+NCR^-$ and NCR^+ cells, whereas increased gene expression was mainly found in NCR^+ ILC3s (29 genes) and $CCR6^-NCR^-$ ILC3s (23 genes).

Accordingly, most of the genes that were decreased in expression in the CCR6^{-}NCR^{-} subset after Notch signaling deletion were found in NCR^{+} ILC3 clusters (cluster III, 6/10 transcripts), including *Runx1*, *Bcl11b*, *Icos*, and *Dtx1*, and in ILC1 clusters (cluster I, 4/19 transcripts), including *Zbtb16*, *Ets1*, and *Nfil3*. On the other hand, increased gene expression was found in NCR^{-} ILC3 clusters (clusters II and IV), including genes encoding cytokines (*Il-17f* and *Ltb*) or cytokine and chemokine receptors (*Ccr6*, *Ccr8*, *Il-17rb*, and *Cxcr5*). These results suggest that the transcriptional profile of CCR6^{-}NCR^{-} cells from *Il7r*$^{Cre/+}$*Rbpj*$^{fl/+}$ mice was similar to that of NCR^{+} ILC3s in haplosufficient mice and was completely different by inactivation of Notch signaling. Conversely, many of the transcripts that were increased in abundance in CCR6^{-}NCR^{-} cells from *Il7r*$^{Cre/+}$*Rbpj*$^{fl/fl}$ mice were shared with other NCR^{-} ILC3 subsets. The expression of *Id2*, *Gata3*, *AhR*, and *Nfil3*, which are essential for the generation of helper-like ILCs, although present in all ILC subsets *(1-3, 10, 23)*, were substantially decreased by the loss of Notch signaling in CCR6^{-}NCR^{-} cells (fig. S7). *Nfil3* and the Notch-dependent gene *Gata3* were also reduced in expression, whereas the expression of *Tox*, which is important for ILC development (*24*), was not affected (Fig. 6D and fig. S7). *Zbtb16* (which encodes the PLZF protein) is transiently expressed by most ILCs in a Notch-dependent manner (*16*). Accordingly, we found that the expression of *Zbtb16* was decreased in all ILC3 subsets from *Il7r*$^{Cre/+}$*Rbpj*$^{fl/fl}$ mice, statistically significantly decreased in ILC1s (fig. S7).

Finally, we were interested in the expression patterns of *Rorc* and *Tbx21*, both of which are required for the development of NCR^{+} ILC3s *(3, 25, 26)*. *Rorc* expression in ILC3 subsets from *Il7r*$^{Cre/+}$*Rbpj*$^{fl/fl}$ mice was substantially reduced compared to that in ILC3 subsets from *Il7r*$^{Cre/+}$*Rbpj*$^{fl/+}$ mice cells. In comparison, T-bet was highly expressed in ILC1s, and, although it

was also found in *Rbpj*-competent and deficient ILC3s, quantities of the T-bet protein did not exhibit a corresponding reduction in protein abundance than observed for its encoding Tbx21 gene after Notch signaling deletion (Fig. 4, E-G). This apparent discrepancy might be explained by the low abundance of T-bet protein in ILC3s, which prevented its proper quantification (Fig. 4F). These results suggest that $CCR6^{-}NCR^{-}$ cells in which Notch signaling was lost could not give rise to NCR^{+} ILC3s such that, in contrast to Notch signaling–competent cells, they had more genes with a similar transcriptional pattern to that found in $CCR6^{+}CD4^{+}$ and $CCR6^{+}CD4^{-}$ NCR^{-} cells. Hence, the Notch signaling pathway appeared to activate a complete transcriptional program that drove progression of the cells toward an NCR^{+} fate.

Discussion

Intestinal NCR^{-} ILC3s contain the putative NCR^{+} precursors previously suggested to be Notch-dependent *(10-13)*. Intestinal ILC3s are both $Notch1^{+}$ and $Notch2^{+}$, whereas fibroblastic stromal cells in lymph nodes (*27*) and in intestinal Paneth cells (*28*) produce the Notch ligands. ILC3s are more abundant in the small intestine than in the colon (*9*), and a study showed a lower ratio of NCR^{+} cells to NCR^{-} cells in the colon compared to in the small intestine (*29*).

In this study, we demonstrated that the intestinal lamina propria is composed of at least two distinct pools of NCR^{+} ILC3s that differ in their dependency on the Notch pathway. Both a major Notch-dependent and a minor (20%) Notch-independent subsets were found in mice in which the *Notch2* or *Rbpj* loci were ablated in hematopoietic progenitor cells (under either the *Il7r* or *Vav* promoters). These results suggest that the reduction in the number of NCR^{+} ILC3s in *Rbpj*-deficient mice was Notch2-dependent, independent of bystander T cells, and cell-

autonomous, which was confirmed by analysis of competitive mixed bone marrow chimeras. On the other hand, $CCR6^{+}NCR^{-}$ ILC3s, which were largely composed of LTi-like cells, were only mildly affected by the absence of Notch signaling. Thus, we propose a model for the Notch-dependent and Notch-independent differentiation of NCR^{+} ILC3s (Fig. 7). We further obtained evidence for the segregation of Notch-dependent and -independent NCR^{+} subsets in vitro. The analysis of 93 transcripts showed that $CCR6^{-}NCR^{-}$ ILC3 precursors that clustered with NCR^{+} cells in haplosufficient mice were more similar to LTi-like cells in the absence of Notch signaling. Hence, the specific effect of loss of Notch signaling in $CCR6^{-}NCR^{-}$ cells resulted in the absence of a subset that resembles NCR^{+} cells.

The progression from NCR^{-} toward NCR^{+} cells is partly controlled by *AhR* (*10*) and T-bet *(11-13)*. Accordingly, the Notch-independent NCR^{+} subset that we identified still had *Tbx21* and *AhR* mRNAs, albeit at reduced amounts compared to those in the Notch-dependent cell subsets. Previous studies with *Tbx21*$^{-/-}$ mice revealed that the few T-bet–independent NCR^{+} cells showed a reduction in the amount of RORγt (*11*). Consistent with this finding, we observed substantial decreases in *Rorc* mRNA and RORγt protein in both $NCR^{-}CCR6^{-}$ cells and NCR^{+} cells in Notch signaling deficient mice, which suggests a role for Notch in activating the expression of both *Tbx21* and *Rorc*. Whereas *Dtx1* expression was undetectable, *Hes1*, *Tcf7*, *Zbtb16*, *Nfil3*, and *Gata3* transcripts were only partially reduced in abundance in the $CCR6^{-}NCR^{-}$ precursors, which suggests that their expression is regulated in part through an alternative pathway. Because our analyses were performed on populations rather than on single cells, the decreased expression of these genes may rather reflect the absence of the Notch-dependent precursors. Nonetheless, NCR^{+} cells exhibited decreased amounts of *Hes1*, *Tcf7*, *Tbx21*, and *Rorc* transcripts in Notch

signaling–deficient ILCs, which suggests that the Notch-independent generation of NCR^+ ILCs is compatible with reduced amounts of these transcripts.

Gata3 inhibits RORγt expression in ILC3s (*14*), and a 50% reduction in RORγt abundance is sufficient to promote the development of T-bet^+ NCR^+ ILC3s (*14*), presumably through de-repression of *Gata3* expression. Because the expression of both *Gata3* and *Tbx21* was reduced in NCR^- cells, the decrease in RORγt abundance appeared to be attributable to the loss of Notch signaling. In *Tbx21* haploinsufficient mice, NCR^+ ILC3s are decreased in number, and T-bet directly stimulates the expression of *Notch2*, but not *Notch1*, during the development of $NKp46^+$ ILCs (*13*). In our analysis, when Notch signaling was inactivated, both *Notch1* and *Notch2* transcripts were increased in abundance in NCR^+ ILC3s, although the abundance of T-bet was maintained. These results suggest that the Notch signaling pathway also regulates receptor abundance through a negative feedback loop.

It was proposed that Notch presence in ILC3s depends on AhR (*10*). Although decreased in abundance among the NCR^- precursors, *AhR* transcripts were still present in Notch signaling–deficient cell populations, which could explain the maintenance of an AhR-dependent, IL-22–secreting $CD4^-CCR6^+$ population in normal numbers. It thus appears that the coordinated actions of RORγt, T-bet, Gata3, AhR, and Notch on the same target cells maintains the equilibrium between the NCR^- and NCR^+ ILC3 subsets. When one of these co-regulators is perturbed by environmental cues or pathologic conditions, the equilibrium shifts toward another subset, thus explaining the plasticity of ILC3s.

Experiments with NCR^+ cells in vitro showed that $NKp46^+$ ILC3s were more efficiently maintained in the presence than absence of Notch ligands, which suggests that Notch signaling is important for the cell-surface expression of NKp46 or for maintaining it. Conversely, in Notch signaling–deficient conditions, the NK cell markers NKp46 and NKG2D were minimally abundant on the surface of NCR^+ cells. Other cell-surface markers, such as Thy1, cKit, and Sca1, also changed their abundances on ILC3 populations when the Notch signaling pathway was lost, which implies that they are partially regulated by the Notch pathway. Transcripts of genes encoding pro- and anti-apoptotic factors in ILC3s were similarly abundant in the presence or absence of Notch signaling, which suggests that NCR^+ cells do not undergo apoptosis in the absence of Notch. $CCR6^+NCR^-$ ILC3s (LTi-like cells) appeared as a stable population, which was in comparison to NCR^+ ILC3s, which lost RORγt and produced IFN-γ, entering a state known as "ex-ILC3" (*9*, *12*). However, neither enhancement nor abrogation of the Notch signaling pathway alone was sufficient to drive the conversion of ILC3s to ILC1s. The increase in the number of NK cells in mice expressing NICD under the control of the *Ncr1* regulatory sequences was probably because of a specific action of Notch on ILC1s. Indeed, this observation did not correlate with the transition from ILC3s to ILC1s, because the number of NCR^+ ILC3s was stable, the abundance of RORγt ILC3s was normal, and the ILC1 subset decreased as a percentage of type I ILCs.

In mice in which NICD was expressed at the earliest developmental stage of IL-7R precursor, more NCR^- cells received a Notch signal and consequently both the $CCR6^-NCR^-$ and NCR^+ populations were increased in number. In culture, NCR^- cells that originated from NCR^+ cells were detected, and they were more frequent in the absence of Notch signaling, which suggests

that NCR^+ cells may revert to NCR^- cells in the absence of Notch signaling. However, no differences in NCR^- cell numbers were found in vivo in the absence of Notch signaling. Hence, these results suggest that *Ncr1* is a direct target of Notch in ILC3s and is required to maintain the NCR^+ identity of the Notch-dependent cell subset. As observed in vitro, the cell-surface expression of NKp46 could be transient on ILC3s, which implies that the NCR^- cell population could contain some "ex-NCR^+" cells. Only a fate map mouse model tracing the $NKp46^+$ cells could determine if the reversion of NCR^+ cells to NCR^- ILC3s is a common event in the intestine. However, we consider that process to be unlikely because a decrease in *Nkp46* expression in the absence of Notch signaling should have revealed an enrichment, rather than a reduction, of the NCR^+ transcriptional signature among the $CCR6^-NCR^-$ population in Notch signaling–deficient mice.

In comparison to previous studies, the mouse model reported here exhibits an inactivation of the Notch signaling pathway that is restricted to the lymphoid compartment and does not affect the Notch2-dependant DC subsets that deliver regulatory cytokines to ILCs. Under steady-state conditions, ILC3s support intestinal homeostasis through such diverse mechanisms as IL-22 secretion to control intestinal microbiota (*30*) or GM-CSF secretion, which preserves the tolerogenic function of intestinal DCs (*31*). We report that Notch signaling–deficient ILC3 subsets have quantitative differences in their secretory capacities that could reinforce or challenge their steady-state functions. Indeed, in Notch signaling–deficient ILC3 subsets, the production of IL-17F, IL-22, and Csf2 was increased compared to that of their Notch signaling–sufficient counterparts, whereas the production of IFN-γ was unaffected. Notch signaling–deficient NCR^+ ILC3s that also had lower amounts of cell-surface NCR markers may have

different functions during infection and inflammation. In conclusion, our study reveals that the Notch2 canonical signaling pathway regulates both the plasticity and function of adult ILC3s.

Materials and Methods

Mice

Il7r^{Cre}*Rosa26*^{YFP} mice [kindly provided by H-R Rodewald, German cancer research center Heidelberg, (*32*)] were crossed with *Rbpj*^{tm1Hon} mice (*33*) (*Il7r*$^{Cre/+}$*Rbpj*$^{fl/+}$*Rosa26*^{YFP}), Notch2 mice (*Il7r*$^{Cre/+}$ *Notch2*$^{fl/+}$ *Rosa26*^{YFP}) (*34*), or NICD mice (*Il7r*$^{Cre/+}$*Rosa26*$^{NICD/+}$) (*35*). *Vav*^{Cre} and *Ncr1*^{Cre}*Rosa26*$^{NICD/+}$ mice were kindly provided by C. Vosshenrich. All animal experiments were approved by the Pasteur Institute Safety Committee in accordance with French Agriculture ministry and the EU guidelines.

Cell preparation

Fetal liver, bone marrow, thymic lobes, spleens, and lamina propria lymphocytes (LPLs) were harvested, dissociated, and resuspended in Hanks' balanced-salt solution (HBSS) supplemented with 1% fetal calf serum (FCS, Gibco). Fetal liver, bone marrow, and spleen cells were depleted of Lineage$^+$ (lin$^+$) cells by staining with biotinylated-conjugated antibodies specific for lineage markers (for bone marrow cells, these include: CD3ε, CD5, CD8α, CD11c, CD19, Ter119, Gr-1, NK1.1, TCRβ, and TCRδ; for spleen cells, these include: CD3ε, CD5, CD8α, CD19, Ter119, Gr-1, TCRβ, and TCRδ), followed by incubation with streptavidin microbeads (Miltenyi Biotec). Depletion was performed on LS+MACS columns (Miltenyi Biotec) from which the negative fraction was recovered. To isolate LPLs, the small bowel was flushed with phosphate-buffered saline (PBS) and the conjunctive tissue and Peyer's patches were carefully removed. The

intestine was opened and cut into 1-cm pieces. To eliminate epithelial cells and intra-epithelial lymphocytes, these fragments were incubated at 37°C in 50 ml of RPMI 1640 (Gibco) containing 10% FCS and 10 mM Hepes buffer under strong agitation for 30 min, which was followed by vortex treatment for 4 min. For LPL isolation, the remaining fragments were incubated in identical medium to which was added type VIII collagenase (0.5 mg/ml, Sigma) and were shaken for 30 min at 37°C. To complete digestion, the suspension was repeatedly passed through a 10-ml syringe for 5 min and then filtered through a 40-µm cell strainer (BD Bioscience) and collected by centrifugation. The cell pellet was re-suspended in 44% Percoll (GE Healthcare), laid over 67% Percoll, and centrifuged at 600*g* for 20 min at 20°C. Cells at the interface were collected, washed in HBSS containing 1% FCS, and recovered.

Flow cytometry and cell sorting

Flow cytometry data were acquired with a FACS Canto II or LSR Fortessa flow cytometer (Becton Dickinson) and analyzed with FlowJo software (TreeStar). Dead cells were eliminated by exclusion with propidium iodide. Cells were stained intracellularly after permeabilization and fixation with Foxp3 Permeabilization/Fixation Concentrate and Diluent (eBioscience). Cells were then incubated for 5 min with DAPI (4,6-diamidino-2-phenylindol; Invitrogen). LPL cells were purified with a FACS Aria III (Becton Dickinson). Cells were recovered in tubes or in 96-well qPCR plates for gene expression analysis.

Antibodies

All antibodies were from BD Biosciences, eBioscience, Biolegend, Cell Signaling Technologies, or R&D Systems. Antibodies were biotinylated or conjugated to fluorochromes (FITC, PE,

PECy5, PerCPCy5.5, PECy7, APC, AlexaFluor647, APCCy7, Pacific Blue, BV421, eFluor450, V500, BV605, BV655, BV700, BV786) and were specific for the following mouse antigens: Ly76 (TER-119), Gr-1 (RB6-8C5), CD11c (HL3), CD3ε (145-2C11), CD5 (53-7.3), CD19 (6D5), NK1.1 (PK136), IL-7Rα (A7R34), c-Kit (2B8), Sca-1 (D7), RORγt (AFKJS-9), $\alpha_4\beta_7$ (DATK32), Flt3 (A2F10), Ly6D (48-H4), CD8 (53-6.7), TCRβ (H57-597), TCRδ (GL3), CCR6 (29-2L17), CD4 (GK1.5), CD25 (PC61), CD44 (IM7), Thy1.2 (53-2.1), NKp46 (29A1.4), GATA-3 (L50-823), ICOS (C398.4A), Ly49 CIFH (14B11), IFN-γ (XMG1.2), IL-22 (1H8PWSR), T-bet (eBio4B10), CD27 (LG.3A10), T1/ST2 (DIH9), CD45.1 (A20), CD45.2 (104), CD23 (B3B4), IL-17A (TC11.18H10.1), CD49a (HMa1), CD49b (DX5), NKG2D (CX5), and CD21 (7E9). Antibody against human Ki67 (B56) was obtained from BD Pharmingen.

Cell culture

All experiments were performed in 96-wells plates at 37°C and 5% CO_2 and in culture medium consisting of OptiMEM, 10% (vol/vol) FCS, penicillin (100 U/ml), streptomycin (100 μg/ml), and 50 μM 2-mercaptoethanol (Gibco). OP9 and OP9-DL4 stromal cells were seeded into 96-well plates. The culture medium was supplemented with saturating amounts of c-Kit ligand, Flt3 ligand, IL-2, and IL-7. The presence of ILC3 subsets was assayed by flow cytometry analyses for the expression of NKp46, RORγt, CCR6 and CD4 proteins among cultured cells after 4 days on OP9 or OP9-DL4 cells.

Chimeric reconstitution

Recipient Ly5.1 mice were sub-lethally irradiated (800rad) before injection. Fetal liver progenitors ($Lin^-IL\text{-}7R\alpha^-cKit^{hi}Sca\text{-}1^+$) cells were sorted from donor Ly5.2 or competitor Ly5.1 ×

Ly5.2 E15 embryos and then mixed at 1:1 ratio for reinjection. Additionally, protective congenic bone marrow cells (1 x 10^6 T cell–depleted Ly5.1 bone marrow cells) in PBS were also injected at the same time into the retro-orbital vein. Reconstituted mice were analyzed after 8 weeks. Cells from the recipient mice were $CD45.1^+CD45.2^-$, whereas competitor cells (WT B6) were $CD45.1^+CD45.2^+$, and *Rbpj*-deficient or *Rbpj*-sufficient donor cells were $CD45.1^-CD45.2^+$.

RT-PCR analysis

Cells were sorted in RLT buffer (Qiagen) containing 2-mercaptoethanol (Sigma) and were frozen at -80°C. RNA was obtained with an RNeasy Micro Kit (Qiagen), and cDNA was obtained with the PrimeScript RT Reagent Kit (Takara). A 7300 Real-Time PCR System (Applied Biosystem) and Taqman technology (Applied Biosystem) or SYBRGreen Technology (Qiagen) were used for quantitative reverse transcriptase polymerase chain reaction (RT-PCR) analysis. A bilateral unpaired Student's *t*-test was used for statistical analysis. The following primers were from SA Biosciences: *Il7f* (PPM05398E), *Il22* (PPM481A), and *Gapdh* (PPM02946E). The following primers were from Applied Biosystems: *Il1r1* (Mm_00434237_m1), *Il23r* (Mm_00519943_m1), *Csf2* (Mm_01290062_m1), *Ifng* (Mm_01168134_m1), *Casp3* (Mm_01195085_m1), *Casp9* (Mm_00516563_m1), *Bcl2* (Mm_00477631_m1), *Bcl2cl1* (Mm_00427783_m1), *Bcl2cl11* (Mm_00432359_m1), *Birc3* (Mm_01168413_m1), *Bik* (Mm_00476123_m1), *Hprt* (Mm_00446968_m1), *Actb* (Mm_02619580_g1).

Multiplex RT-PCR analysis

Total RNA from the appropriate cell populations was extracted as previously described (*19*) and mixed in 10 µl of CellsDirect One-Step qRT-PCR Kit (Life Technologies), containing a mixture

of diluted primers (0.05× final concentration). See table S1 for sequences. Pre-amplified cDNA (22 cycles) was obtained according to the manufacturer's instructions and was diluted 1:5 in TE buffer (pH 8, Ambion). The sample mixture was as follows: diluted cDNA (2.9 µl), Sample Loading Reagent (0.32 µl, Fluidigm), and either Taqman Universal PCR Master Mix (3.5 µl, Applied Biosystems) or Solaris qPCR Low ROX Master Mix (3.5 µl, GE Dharmacon). The assay mixture was as follows: Assay Loading Reagent (Fluidigm) and either Taqman (Applied Biosystem) or Solaris (GE Dharmacon). A 96.96 dynamic array integrated fluidic circuit (IFC, Fluidigm) was primed with control line fluid, and the chip was loaded with assays (either Taqman or Solaris) and samples with an HX IFC controller (Fluidigm). The experiments were run on a Biomark HD (Fluidigm) for 40 cycles. Samples that did not express at least one of three housekeeping genes (*Actb*, *Gapdh*, or *Hprt*) and genes that were present in less than 5% of the wells (except for *Dtx1*, *Pax5*, *Ebf1* and *Rag2*) were removed from the analysis. Gene expression was assessed by the $2^{-\Delta Ct}$ method.

Statistical analysis

Statistical analysis was performed with the Mann Whitney nonparametric test where appropriate. These tests were performed with Prism software (GraphPad). Graphs containing error bars show means ± SEM. Statistical significance is represented as follows: $*P < 0.05$, $**P < 0.01$, $***P < 0.001$.

Supplementary Materials

Fig. S1. *Rbpj* is efficiently deleted in IL-7Rα^+ CLPs by Cre recombinase.
Fig. S2. Notch2 signaling is specifically required for both NCR$^+$ and NCR$^-$ ILC3s.
Fig. S3. Analysis of cytokine secretion and receptors in Notch signaling–competent (*Il7r*$^{Cre/+}$*Rbpj*$^{fl/+}$) and deficient (*Il7r*$^{Cre/+}$*Rbpj*$^{fl/fl}$) mice.

Fig. S4. Expression of *Gata3* and *Il7ra* in ILC3 subsets in the presence or absence of Notch signaling.
Fig. S5. The expression of genes encoding pro-apoptotic proteins in ILC3 subsets is unchanged by the loss of Notch signaling.
Fig. S6. Analysis of ILC3 and ILC1 subsets in $Ncr1^{Cre/+}Rosa26^{NICD/+}$ mice.
Fig. S7. Analysis of transcription factors expressed from ILC3 and ILC1 subsets in Notch signaling–competent ($Il7r^{Cre/+}Rbpj^{fl/+}$) and -deficient ($Il7r^{Cre/+}Rbpj^{fl/fl}$) mice .
Table S1. *P* values for the differential expression of 92 genes between $Il7r^{Cre/+}Rbpj^{fl/+}$ and $Il7r^{Cre/+}Rbpj^{fl/fl}$ ILC3 subsets (respectively, NCR^+, $CCR6^+$ NCR^- and $CCR6^-$ NCR^- subsets).

References and Notes

1. Y. Yokota, A. Mansouri, S. Mori, S. Sugawara, S. Adachi, S. Nishikawa, P. Gruss, Development of peripheral lymphoid organs and natural killer cells depends on the helix-loop-helix inhibitor Id2. *Nature* **397**, 702-706 (1999).
2. K. Moro, T. Yamada, M. Tanabe, T. Takeuchi, T. Ikawa, H. Kawamoto, J. Furusawa, M. Ohtani, H. Fujii, S. Koyasu, Innate production of T(H)2 cytokines by adipose tissue-associated c-Kit(+)Sca-1(+) lymphoid cells. *Nature* **463**, 540-544 (2010).
3. N. Satoh-Takayama, , S. Lesjean-Pottier, P. Vieira, S. Sawa, G. Eberl, C. A. Vosshenrich, J. P. Di Santo, IL-7 and IL-15 independently program the differentiation of intestinal CD3-NKp46+ cell subsets from Id2-dependent precursors. *J Exp Med* **207**, 273-280 (2010).
4. N. Serafini, C. A. Vosshenrich, J. P. Di Santo, Transcriptional regulation of innate lymphoid cell fate. *Nat Rev Immunol* **15**, 415-428 (2015).
5. M. L. Robinette, A. Fuchs, V. S. Cortez, J. S. Lee, Y. Wang, S. K. Durum, S. Gilfillan, M. Colonna, Transcriptional programs define molecular characteristics of innate lymphoid cell classes and subsets. *Nat Immunol* **16**, 306-317 (2015).
6. R. E. Mebius, P. Rennert, I. L. Weissman, Developing lymph nodes collect CD4+CD3- LTbeta+ cells that can differentiate to APC, NK cells, and follicular cells but not T or B cells. *Immunity* **7**, 493-504 (1997).
7. G. Eberl, S. Marmon, M. J. Sunshine, P. D. Rennert, Y. Choi, D. R. Littman, An essential function for the nuclear receptor RORgamma(t) in the generation of fetal lymphoid tissue inducer cells. *Nat Immunol* **5**, 64-73 (2004).
8. S. Sawa, M. Cherrier, M. Lochner, N. Satoh-Takayama, H. J. Fehling, F. Langa, J. P. Di Santo, G. Eberl, Lineage relationship analysis of RORgammat+ innate lymphoid cells. *Science* **330**, 665-669 (2010).
9. C. Vonarbourg A. Mortha, V. L. Bui, P. P. Hernandez, E. A. Kiss, T. Hoyler, M. Flach, B. Bengsch, R. Thimme, C. Holscher, M. Honig, U. Pannicke, K. Schwarz, C. F. Ware, D. Finke, A. Diefenbach, Regulated expression of nuclear receptor RORgammat confers distinct functional fates to NK cell receptor-expressing RORgammat(+) innate lymphocytes. *Immunity* **33**, 736-751 (2010).
10. J. S. Lee, M. Cella, K. G. McDonald, C. Garlanda, G. D. Kennedy, M. Nukaya, A. Mantovani, R. Kopan, C. A. Bradfield, R. D. Newberry, M. Colonna, AHR drives the development of gut ILC22 cells and postnatal lymphoid tissues via pathways dependent on and independent of Notch. *Nat Immunol* **13**, 144-151 (2012).
11. G. Sciume, K. Hirahara, H. Takahashi, A. Laurence, A. V. Villarino, K. L. Singleton, S. P. Spencer, C. Wilhelm, A. C. Poholek, G. Vahedi, Y. Kanno, Y. Belkaid, J. J. O'Shea, Distinct requirements for T-bet in gut innate lymphoid cells. *J Exp Med* **209**, 2331-2338 (2012).

12. C. S. Klose, E. A. Kiss, V. Schwierzeck, K. Ebert, T. Hoyler, Y. d'Hargues, N. Goppert, A. L. Croxford, A. Waisman, Y. Tanriver, and A. Diefenbach., A T-bet gradient controls the fate and function of CCR6-RORgammat+ innate lymphoid cells. *Nature* **494**, 261-265 (2013).
13. L. C. Rankin, J. R. Groom, M. Chopin, M. J. Herold, J. A. Walker, L. A. Mielke, A. N. McKenzie, S. Carotta, S. L. Nutt, G. T. Belz., The transcription factor T-bet is essential for the development of NKp46+ innate lymphocytes via the Notch pathway. *Nat Immunol* **14**, 389-395 (2013).
14. C. Zhong, K. Cui, C. Wilhelm, G. Hu, K. Mao, Y. Belkaid, K. Zhao, and J. Zhu, Group 3 innate lymphoid cells continuously require the transcription factor GATA-3 after commitment. *Nat Immunol* **17**, 169-178 (2016).
15. T. Ebihara, C. Song, S. H. Ryu, B. Plougastel-Douglas, L. Yang, D. Levanon, Y. Groner, M. D. Bern, T. S. Stappenbeck, M. Colonna, T. Egawa, and W. M. Yokoyama, Runx3 specifies lineage commitment of innate lymphoid cells. *Nat Immunol* **16**, 1124-1133 (2015).
16. M. G. Constantinides, B. D. McDonald, P. A. Verhoef, A. Bendelac, A committed precursor to innate lymphoid cells. *Nature* **508**, 397-401 (2014).
17. C. S. Klose, M. Flach, L. Mohle, L. Rogell, T. Hoyler, K. Ebert, C. Fabiunke, D. Pfeifer, V. Sexl, D. Fonseca-Pereira, R. G. Domingues, H. Veiga-Fernandes, S. J. Arnold, M. Busslinger, I. R. Dunay, Y. Tanriver, and A. Diefenbach, Differentiation of type 1 ILCs from a common progenitor to all helper-like innate lymphoid cell lineages. *Cell* **157**, 340-356 (2014).
18. S. H. Wong, J. A. Walker, H. E. Jolin, L. F. Drynan, E. Hams, A. Camelo, J. L. Barlow, D. R. Neill, V. Panova, U. Koch, F. Radtke, C. S. Hardman, Y. Y. Hwang, P. G. Fallon, A. N. McKenzie, Transcription factor RORalpha is critical for nuocyte development. *Nat Immunol* **13**, 229-236 (2012).
19. C. Possot, S. Schmutz, S. Chea, L. Boucontet, A. Louise, A. Cumano, R. Golub, Notch signaling is necessary for adult, but not fetal, development of RORgammat(+) innate lymphoid cells. *Nat Immunol* **12**, 949-958 (2011).
20. K. L. Lewis, M. L. Caton, M. Bogunovic, M. Greter, L. T. Grajkowska, D. Ng, A. Klinakis, I. F. Charo, S. Jung, J. L. Gommerman, I. I. Ivanov, K. Liu, M. Merad, and B. Reizis, Notch2 receptor signaling controls functional differentiation of dendritic cells in the spleen and intestine. *Immunity* **35**, 780-791 (2011).
21. Rothenberg, E. V. 2012. Transcriptional drivers of the T-cell lineage program. *Curr Opin Immunol* 24: 132-138.
22. E. E. Schmidt, U. Schibler, High accumulation of components of the RNA polymerase II transcription machinery in rodent spermatids. *Development* **121**, 2373-2383 (1995).
23. T. Hoyler, C. S. Klose, A. Souabni, A. Turqueti-Neves, D. Pfeifer, E. L. Rawlins, D. Voehringer, M. Busslinger, A. Diefenbach, The transcription factor GATA-3 controls cell fate and maintenance of type 2 innate lymphoid cells. *Immunity* **37**, 634-648 (2012).
24. C. R. Seehus, P. Aliahmad, B. de la Torre, I. D. Iliev, L. Spurka, V. A. Funari, J. Kaye, The development of innate lymphoid cells requires TOX-dependent generation of a common innate lymphoid cell progenitor. *Nat Immunol* **16**, 599-608 (2015).
25. N. Satoh-Takayama, C. A. Vosshenrich, S. Lesjean-Pottier, S. Sawa, M. Lochner, F. Rattis, J. J. Mention, K. Thiam, N. Cerf-Bensussan, O. Mandelboim, G. Eberl, J. P. Di Santo, Microbial flora drives interleukin 22 production in intestinal NKp46+ cells that provide innate mucosal immune defense. *Immunity* **29**, 958-970 (2008).

26. L. A. Mielke, J. R. Groom, L. C. Rankin, C. Seillet, F. Masson, T. Putoczki, and G. T. Belz, TCF-1 controls ILC2 and NKp46+RORgammat+ innate lymphocyte differentiation and protection in intestinal inflammation. *J Immunol* **191**, 4383-4391 (2013).
27. N. Fasnacht, H. Y. Huang, U. Koch, S. Favre, F. Auderset, Q. Chai, L. Onder, S. Kallert, D. D. Pinschewer, H. R. MacDonald, F. Tacchini-Cottier, B. Ludewig, S. A. Luther, F. Radtke., Specific fibroblastic niches in secondary lymphoid organs orchestrate distinct Notch-regulated immune responses. *J Exp Med* **211**, 2265-2279 (2014).
28. T. Sato, J. H. van Es, H. J. Snippert, D. E. Stange, R. G. Vries, M. van den Born, N. Barker, N. F. Shroyer, M. van de Wetering, H. Clevers. 2011, Paneth cells constitute the niche for Lgr5 stem cells in intestinal crypts. *Nature* **469**, 415-418 (2011).
29. C. Song, J. S. Lee, S. Gilfillan, M. L. Robinette, R. D. Newberry, T. S. Stappenbeck, M. Mack, M. Cella, M. Colonna, Unique and redundant functions of NKp46+ ILC3s in models of intestinal inflammation. *J Exp Med* **212**, 1869-1882 (2015).
30. G. F. Sonnenberg, D. Artis, Innate lymphoid cell interactions with microbiota: implications for intestinal health and disease. *Immunity* **37**, 601-610 (2012).
31. A. Mortha, A. Chudnovskiy, D. Hashimoto, M. Bogunovic, S. P. Spencer, Y. Belkaid, M. Merad, Microbiota-dependent crosstalk between macrophages and ILC3 promotes intestinal homeostasis. *Science* **343**, 1249288-7 (2014).
32. S. M. Schlenner, V. Madan, K. Busch, A. Tietz, C. Laufle, C. Costa, C. Blum, H. J. Fehling, H. R. Rodewald, Fate mapping reveals separate origins of T cells and myeloid lineages in the thymus. *Immunity* **32**, 426-436 (2010).
33. H. Han, K. Tanigaki, N. Yamamoto, K. Kuroda, M. Yoshimoto, T. Nakahata, K. Ikuta, T. Honjo., Inducible gene knockout of transcription factor recombination signal binding protein-J reveals its essential role in T versus B lineage decision. *Int Immunol* **14**, 637-645 (2002).
34. B. McCright, J. Lozier, T. Gridley, Generation of new Notch2 mutant alleles. *Genesis* **44**, 29-33 (2006).
35. L. C. Murtaugh, B. Z. Stanger, K. M. Kwan, D. A. Melton, Notch signaling controls multiple steps of pancreatic differentiation. *Proc Natl Acad Sci U S A* **100**, 14920-14925(2003).

Acknowledgments: We thank A. Bandeira for critical reading of the manuscript and S. Bechet for help with illustrations. We acknowledge the Center for Human Immunology and the Cytometry platform at Institut Pasteur for support. We thank H-R Rodewald, (German cancer research center, Heidelberg), for the *Il7r*^{Cre}*Rosa26*^{YFP} mice. **Funding:** This work was supported by the Pasteur Institute, Institut National de la Santé et de la Recherche Médicale (INSERM), Université Paris Diderot, and by the Ministère de la Recherche to S.C and T.V.; the Association pour la Recherche sur le Cancer to S.C. and R.G.; the REVIVE Future Investment Program and the Agence Nationale de Recherche ANR (Grant "Twothyme") to A.C.; the Ligue Nationale contre le Cancer to J.P.D. and T.V.; the Agence Nationale de la Recherche ANR (Grant "Myeloten") to R.G.; and the Institut National du Cancer (Grant «Role of the immune microenvironment during liver carcinogenesis») to R.G. and the USPC (Grant «Mucocell»).
Author contributions: S.C. performed most of the experiments and analyzed data; T.P. performed and analyzed experiments and prepared figures; M.P. performed and analyzed experiments; T.V. performed experiments with the *Ncr1*^{Cre}NICD mice; E.G.B. performed the mouse genotyping; D.G.G. supervised experiments with lamina propria cells and contributed to the writing of the manuscript; C.V. generated the *Ncr1*^{Cre} mice; J.P.D. and A.C. contributed to the writing of the manuscript; and R.G. directed the research, designed experiments, analyzed

data, and wrote the manuscript. **Competing interests:** The authors declare that they have no competing interests.

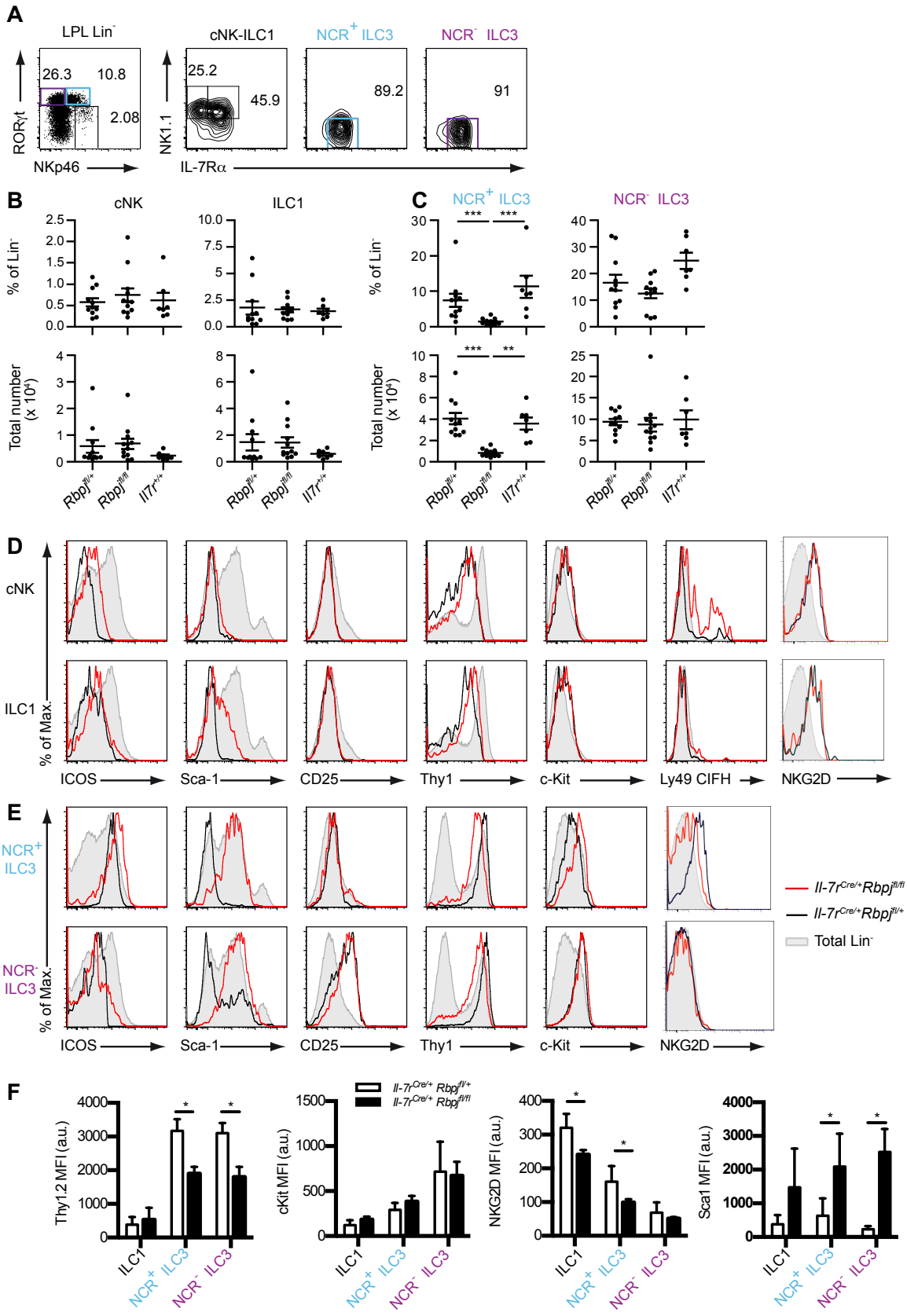
A
LPL Lin-
cNK-ILC1
NCR+ ILC3
NCR- ILC3
26.3
10.8
2.08
25.2
45.9
89.2
91
RORγt
NKp46
NK1.1
IL-7Rα
B
cNK
ILC1
% of Lin-
Total number (x 10⁴)
Rbpj fl/+
Rbpj fl/fl
Il7r+/+
C
NCR+ ILC3
NCR- ILC3
***
**
D
cNK
ILC1
% of Max.
ICOS
Sca-1
CD25
Thy1
c-Kit
Ly49 CIFH
NKG2D
E
NCR+ ILC3
NCR- ILC3
Il-7rCre/+Rbpjfl/fl
Il-7rCre/+Rbpjfl/+
Total Lin-
F
Thy1.2 MFI (a.u.)
cKit MFI (a.u.)
NKG2D MFI (a.u.)
Sca1 MFI (a.u.)
ILC1
NCR+ ILC3
NCR- ILC3

Fig. 1. Loss of Notch signaling alters the homeostasis of intestinal ILC3 subsets. (**A**) Flow cytometric analysis of lamina propria lymphocytes (LPLs) from C57Bl/6 mice. Lin^- cells were defined according to the presence of RORγt, IL-7Rα, and NKp46 into cNK cells ($ROR\gamma t^-$ $NKp46^+NK1.1^+IL\text{-}7R\alpha^-$), ILC1s ($ROR\gamma t^-NKp46^+NK1.1^+IL\text{-}7R\alpha^+$), NCR^+ ILC3s ($ROR\gamma t^+NKp46^+IL\text{-}7R\alpha^+$), and NCR^- ILC3s ($ROR\gamma t^+NKp46^-NK1.1^-IL\text{-}7R\alpha^+$). (**B**) Percentages (top) and total numbers (bottom) of cNK cells and ILC1s from *Il-7r*$^{Cre/+}$*Rbpj*$^{fl/+}$, *Il-7r*$^{Cre/+}$*Rbpj*$^{fl/fl}$, and *Il-7r*$^{+/+}$*Rbpj*$^{fl/+}$ mice. (**C**) Percentages (top) and total numbers (bottom) of NCR^+ ILC3s and NCR^- ILC3s from *Il-7r*$^{Cre/+}$*Rbpj*$^{fl/+}$, *Il-7r*$^{Cre/+}$*Rbpj*$^{fl/fl}$, and *Il-7r*$^{+/+}$*Rbpj*$^{fl/+}$ mice. (**D**) Flow cytometric analysis of the amounts of Icos, Sca-1, CD25, Thy1, c-Kit, and Ly49 CIFH in cNK cells and ILC1s from *Il-7r*$^{Cre/+}$ *Rbpj*$^{fl/+}$ mice (black) and *Il-7r*$^{Cre/+}$ *Rbpj*$^{fl/fl}$ (red) mice compared to those in total Lin^- cells (gryy). (**E**) Flow cytometric analysis of the amounts of Icos, Sca-1, CD25, Thy1, c-Kit, and Ly49 CIFH in NCR+ ILC3s and NCR– ILC3s from *Il-7r*$^{Cre/+}$ *Rbpj*$^{fl/+}$ mice (black) and *Il-7r*$^{Cre/+}$ *Rbpj*$^{fl/fl}$ (red) mice compared to those in total Lin^- cells (gray). (**F**) Mean fluorescence intensities (MFIs) of Thy1, c-Kit, NKG2D, and Sca1 for ILC1s, NCR^+ ILC3s, and NCR^- ILC3s from *Il-7r*$^{Cre/+}$ *Rbpj*$^{fl/+}$ mice (white) and *Il-7r*$^{Cre/+}$ *Rbpj*$^{fl/fl}$ (black) mice. a.u., arbitrary units. Data are representative of at least three independent experiments with at least three mice of each genotype analyzed per experiment. Data in (B), (C), and (F) are means ± SEM of three independent experiments, with three mice of each genotype analyzed per experiment. Data points in (B) and (C) represent individual mice. $^*P < 0.05$; $^{**}P < 0.01$; $^{***}P < 0.001$ by Mann Whitney test.

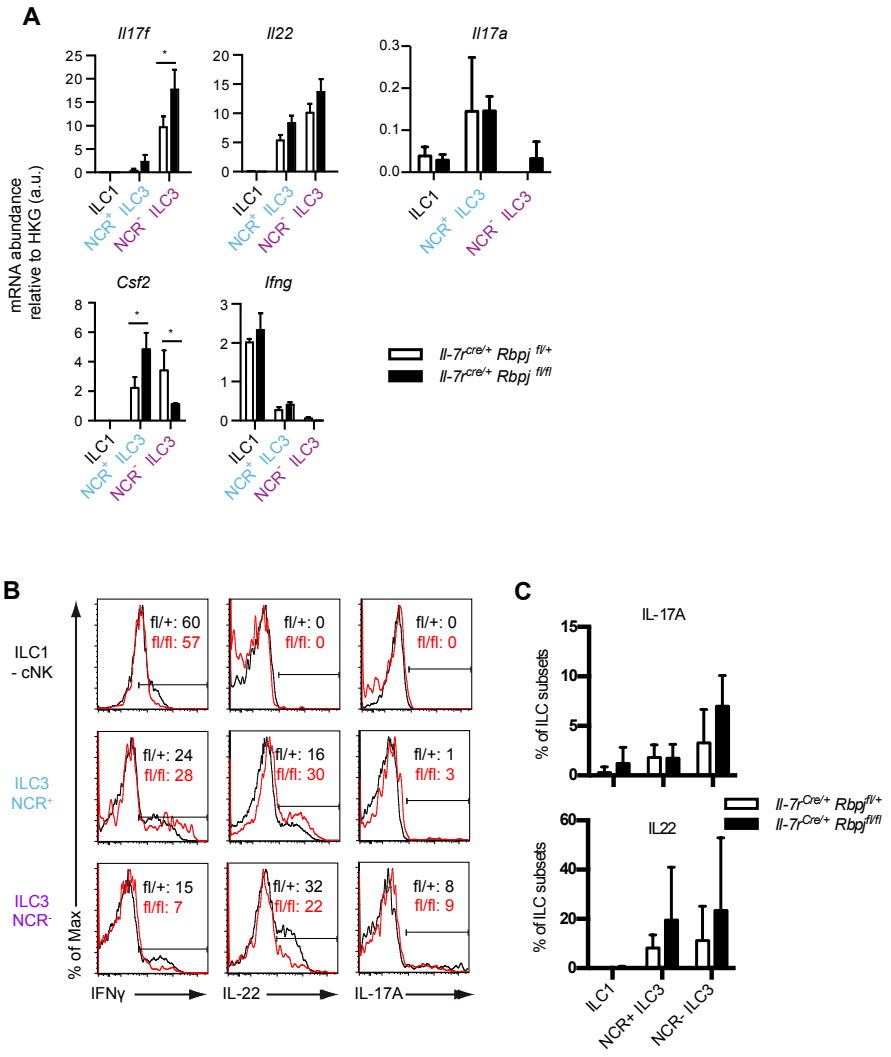
A
Il17f
Il22
Il17a
Csf2
Ifng
mRNA abundance relative to HKG (a.u.)
ILC1
NCR+ ILC3
NCR- ILC3
Il-7rcre/+ Rbpj fl/+
Il-7rcre/+ Rbpj fl/fl
B
ILC1 - cNK
ILC3 NCR+
ILC3 NCR-
fl/+: 60
fl/fl: 57
fl/+: 0
fl/fl: 0
fl/+: 0
fl/fl: 0
fl/+: 24
fl/fl: 28
fl/+: 16
fl/fl: 30
fl/+: 1
fl/fl: 3
fl/+: 15
fl/fl: 7
fl/+: 32
fl/fl: 22
fl/+: 8
fl/fl: 9
% of Max
IFNγ
IL-22
IL-17A
C
IL-17A
IL22
% of ILC subsets
Il-7rCre/+ Rbpjfl/+
Il-7rCre/+ Rbpjfl/fl
ILC1
NCR+ ILC3
NCR- ILC3

Fig. 2. Changes in the cytokine profiles of ILC3 subsets from mice deficient in Notch signaling. (**A**) Quantitative RT-PCR analysis of the relative abundances of *Il17f*, *Il22*, *Il17a*, *Csf2*, and *Ifng* mRNAs in ILC1, NCR^+ ILC3, and NCR^- ILC3 subsets (as defined in Fig. 1A) from $Il\text{-}7r^{Cre/+}Rbpj^{fl/+}$ mice (white) and $Il\text{-}7r^{Cre/+}Rbpj^{fl/fl}$ mice (black). The abundances of the indicated mRNAs are presented relative to the average abundances of mRNAs of housekeeping genes. Data are means ± SEM of three independent experiments, with three mice of each genotype analyzed per experiment. $^{*}P < 0.05$, $^{**}P < 0.01$, $^{***}P < 0.001$ by Mann Whitney test. (**B**) cNK-ILC1, NCR^+ ILC3, and NCR^- ILC3 subsets isolated from $Il\text{-}7r^{Cre/+}\,Rbpj^{fl/+}$ mice (black) and $Il\text{-}7r^{Cre/+}\,Rbpj^{fl/fl}$ mice (red) were treated with PMA (left) or IL-23 (middle and right) and then were analyzed by flow cytometry to determine the relative abundances of IFN-γ (left), IL-22 (middle), and IL-17A (right). Data are representative of two independent experiments. (**C**) Analysis of the percentages of the indicated subsets of cells from $Il\text{-}7r^{Cre/+}\,Rbpj^{fl/+}$ (white bars) and $Il\text{-}7r^{Cre/+}\,Rbpj^{fl/fl}$ mice (black bars) that were positive for IL-17A (top) or IL-22 (bottom) in response to treatment with IL-23. Data are means ± SEM of two independent experiments, with two mice of each genotype analyzed per experiment. Analysis by Mann Whitney test showed that there were no statistically significant differences among the groups.

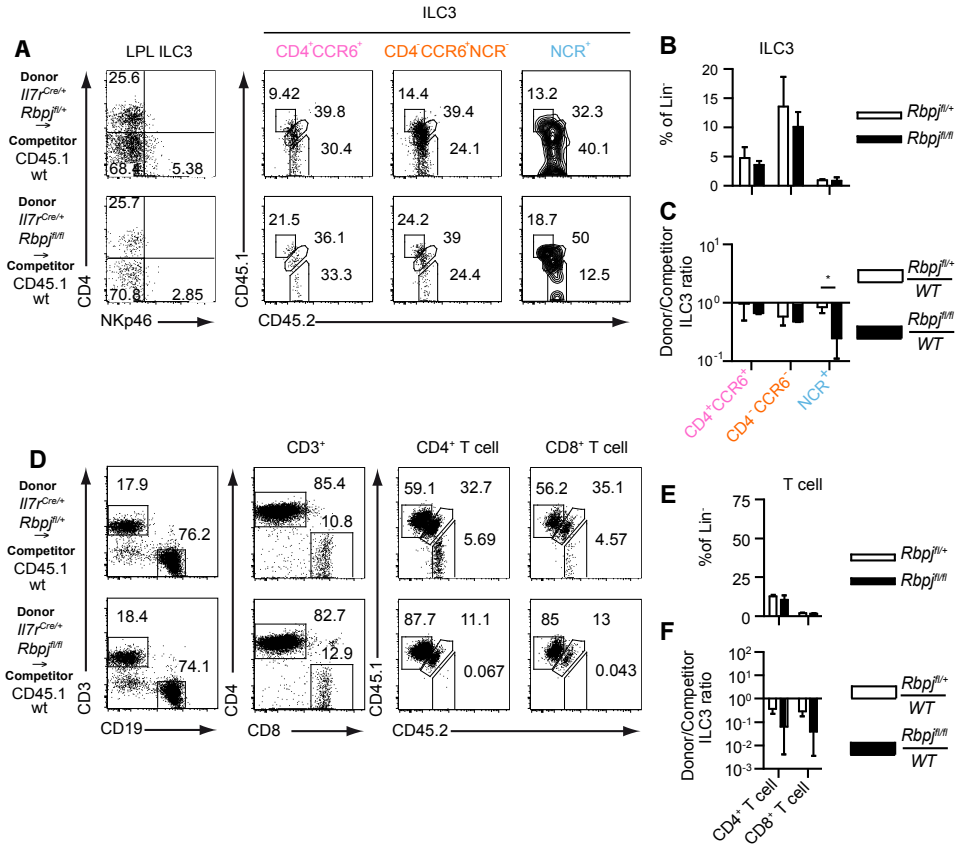
A
LPL ILC3
ILC3
CD4+CCR6+
CD4-CCR6+NCR-
NCR+
Donor
Il7rCre/+
Rbpjfl/+
Competitor
CD45.1
wt
Donor
Il7rCre/+
Rbpjfl/fl
Competitor
CD45.1
wt
25.6
68.4
5.38
25.7
70.8
2.85
CD4
NKp46
9.42
39.8
30.4
14.4
39.4
24.1
13.2
32.3
40.1
21.5
36.1
33.3
24.2
39
24.4
18.7
50
12.5
CD45.1
CD45.2
B
ILC3
% of Lin-
20
15
10
5
0
Rbpjfl/+
Rbpjfl/fl
C
Donor/Competitor
ILC3 ratio
10^1
10^0
10^-1
*
Rbpjfl/+
WT
Rbpjfl/fl
WT
CD4+CCR6+
CD4-CCR6-
NCR+
D
CD3+
CD4+ T cell
CD8+ T cell
Donor
Il7rCre/+
Rbpjfl/+
Competitor
CD45.1
wt
Donor
Il7rCre/+
Rbpjfl/fl
Competitor
CD45.1
wt
17.9
76.2
18.4
74.1
CD3
CD19
85.4
10.8
82.7
12.9
CD4
CD8
59.1
32.7
5.69
87.7
11.1
0.067
56.2
35.1
4.57
85
13
0.043
CD45.1
CD45.2
E
T cell
%of Lin-
75
50
25
0
Rbpjfl/+
Rbpjfl/fl
F
Donor/Competitor
ILC3 ratio
10^2
10^1
10^0
10^-1
10^-2
10^-3
Rbpjfl/+
WT
Rbpjfl/fl
WT
CD4+ T cell
CD8+ T cell

Fig. 3. The disruption of ILC3 homeostasis in Notch signaling–deficient mice is cell-intrinsic. (**A** to **D**) A total of 2000 fetal liver LSK cells from embryonic day 15.5 (E15.5) $CD45.2^+CD45.1^-$ donor mice (either $Il7r^{Cre/+}Rbpj^{fl/+}$ or $Il7r^{Cre/+}Rbpj^{fl/fl}$) and from $CD45.2^+CD45.1^+$ competitor B6 wild-type (WT) mice were injected at a 1:1 ratio into lethally irradiated $CD45.2^-CD45.1^+$ recipient mice, as indicated. The mice were analyzed 8 weeks after reconstitution. (A) Flow cytometric analysis of the ILC3s in the lamina propria of the indicated mice after reconstitution. Lamina propria ILC3s (LPL ILC3s) were assigned, based on their cell-surface expression of CD4, CCR6, and NKp46, into $CD4^+CCR6^+$ NCR^- cells (pink), $CD4^-CCR6^-$ NCR^- cells (orange), and $CD4^-NKp46^-$ NCR^+ cells (blue). (B) Percentages of donor ILC3 subsets from the lamina propria of both type of reconstituted mice (*Il-7r*$^{Cre/+}$ *Rbpj*$^{fl/+}$*: WT* in white or *Il-7r*$^{Cre/+}$ *Rbpj*$^{fl/fl}$*: WT* in black). (C) Donor:competitor ratios of ILC3 subsets [as defined in (A)] after reconstitution from reconstituted mice with *Il-7r*$^{Cre/+}$ *Rbpj*$^{fl/+}$*: WT* (white) or *Il-7r*$^{Cre/+}$ *Rbpj*$^{fl/fl}$*: WT* (black). (D) Flow cytometric analysis of $CD4^+$ T cell (defined as $CD3^+$ $CD4^+$) and $CD8^+$ T cell (defined as $CD3^+$ $CD8^+$) subsets in the spleen of the indicated mice after reconstitution. (E) Percentages of donor $CD4^+$ T cell and $CD8^+$ T cell subsets from the lamina propria of both type of reconstituted mice (*Il-7r*$^{Cre/+}$ *Rbpj*$^{fl/+}$*: WT* in white or *Il-7r*$^{Cre/+}$ *Rbpj*$^{fl/fl}$*: WT* in black). (F) Donor:competitor ratios of $CD4^+$ T cell and $CD8^+$ T cell subsets [as defined in (C)] from reconstituted mice with *Il-7r*$^{Cre/+}$ *Rbpj*$^{fl/+}$*: WT* (white) or *Il-7r*$^{Cre/+}$ *Rbpj*$^{fl/fl}$*: WT* (black). Data are representative of two independent experiments, with four or five mice of each group analyzed per experiment. Data in (B) and (D) are means ± SEM. $^*P < 0.05$, $^{**}P < 0.01$, $^{***}P < 0.001$ by Mann Whitney test.

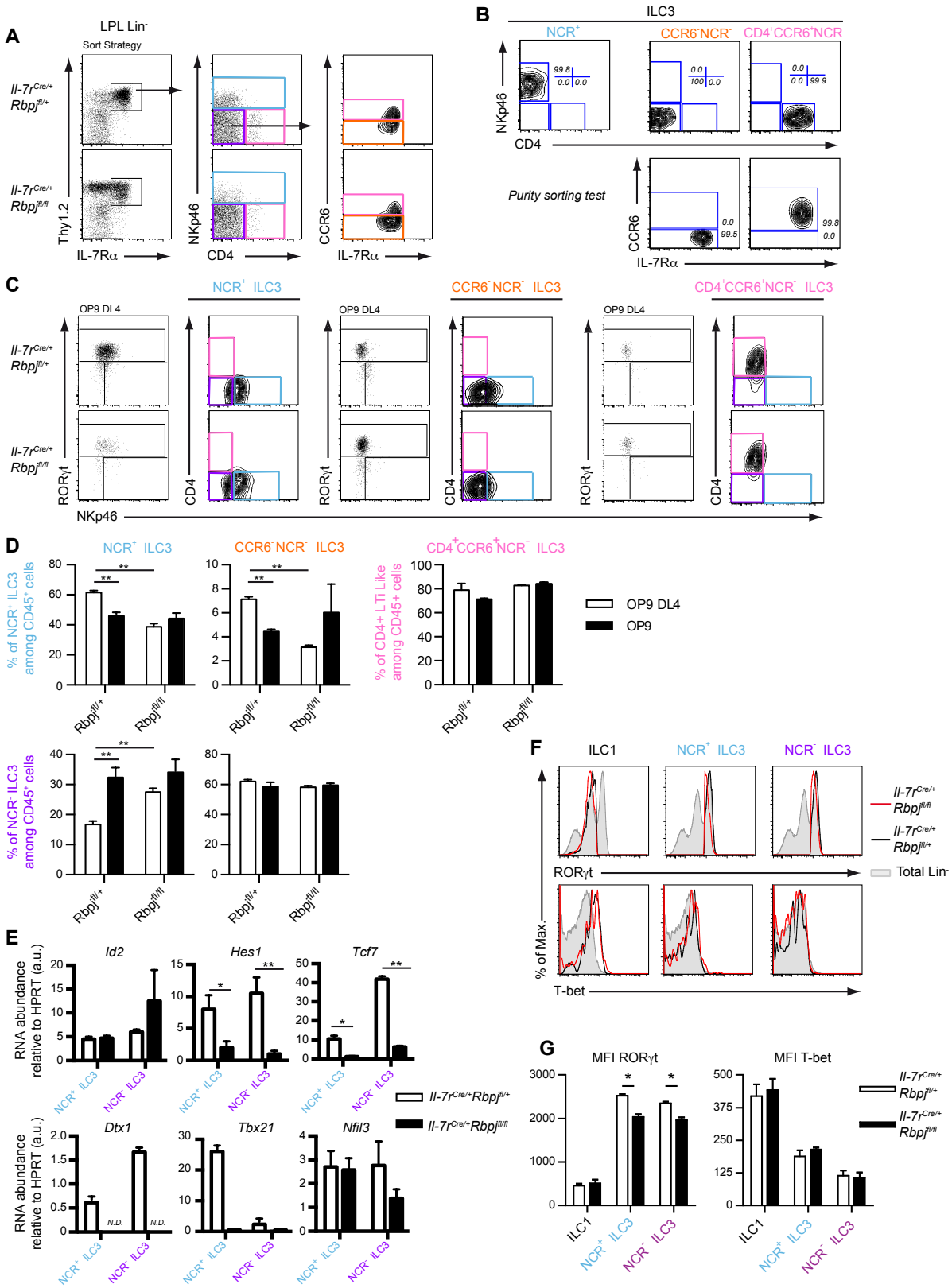
A
LPL Lin-
Sort Strategy
Il-7rCre/+ Rbpjfl/+
Il-7rCre/+ Rbpjfl/fl
Thy1.2
IL-7Rα
NKp46
CD4
CCR6
B
ILC3
NCR+
CCR6-NCR-
CD4+CCR6+NCR-
NKp46
CD4
Purity sorting test
CCR6
IL-7Rα
C
NCR+ ILC3
CCR6-NCR- ILC3
CD4+CCR6+NCR- ILC3
OP9 DL4
RORγt
CD4
NKp46
D
% of NCR+ ILC3 among CD45+ cells
% of CD4+ LTi Like among CD45+ cells
% of NCR- ILC3 among CD45+ cells
OP9 DL4
OP9
E
Id2
Hes1
Tcf7
Dtx1
Tbx21
Nfil3
RNA abundance relative to HPRT (a.u.)
N.D.
F
ILC1
NCR+ ILC3
NCR- ILC3
RORγt
T-bet
% of Max.
Total Lin-
G
MFI RORγt
MFI T-bet

Fig. 4. Notch signaling contributes to the maintenance of NCR$^+$ ILC3s and the conversion of NCR$^-$ ILC3s into NCR$^+$ ILC3s. (**A**) Sorting strategy of NCR$^+$ ILC3s (in blue; Lin$^-$NK1.1$^-$ KLRG1$^-$IL-7Rα$^+$Thy1.2$^+$NKp46$^+$), CCR6$^-$ NCR$^-$ ILC3s (in orange; Lin$^-$NK1.1$^-$KLRG1$^-$IL-7Rα$^+$Thy1.2$^+$NKp46$^-$CCR6$^-$), and CCR6$^+$ NCR$^-$ ILC3s (in pink; Lin$^-$NK1.1$^-$KLRG1$^-$IL-7Rα$^+$Thy1.2$^+$NKp46$^-$CCR6$^+$) from *Il-7r*$^{Cre/+}$ *Rbpj*$^{fl/+}$ mice (top) and *Il-7r*$^{Cre/+}$ *Rbpj*$^{fl/fl}$ mice (bottom). (**B**) Purity sorting test. After sorting, sorted cell populations were analyzed by flow cytometry a second time to check cell populations purity. All sorted cell population purity were superior to 99%. Data in (A) and (B) are representative of at least 3 experiments. (**C**) Flow cytometric analysis of the indicated ILC3 subsets isolated from *Il-7r*$^{Cre/+}$ *Rbpj*$^{fl/+}$ mice (top) and *Il-7r*$^{Cre/+}$ *Rbpj*$^{fl/fl}$ mice (bottom) and cultured for 4 days on OP9-DL4 cells. Data are representative of four independent experiments. (**D**) Analysis of the indicated ILC3 subsets after culture on OP9-DL4 cells (white) or OP9 cells (black) expressed as a percentage of CD45$^+$ cells. Data are means ± SEM of four independent experiments. (**E**) Quantitative RT-PCR analysis of NCR$^+$ ILC3s and NCR$^-$ ILC3s isolated from *Il-7r*$^{Cre/+}$ *Rbpj*$^{fl/+}$ mice (white) and *Il-7r*$^{Cre/+}$ *Rbpj*$^{fl/fl}$ mice (black). The abundances of the indicated mRNAs are presented relative to the average of those of the appropriate housekeeping genes. N.D., not detected. Data are means ± SEM of two independent experiments, with four mice of each genotype analyzed per experiment. (**F**) Flow cytometric analysis of the relative amounts of T-bet in ILC1s, NCR$^+$ ILC3s, and NCR$^-$ ILC3s isolated from *Il-7r*$^{Cre/+}$ *Rbpj*$^{fl/+}$ mice (black) and *Il-7r*$^{Cre/+}$ *Rbpj*$^{fl/fl}$ mice (red) compared to those in total Lin$^-$ cells (gray). Data are representative of three independent experiments. (**G**) Comparison of the MFIs of RORγt and T-bet in the indicated sorted cells isolated from *Il-7r*$^{Cre/+}$ *Rbpj*$^{fl/+}$ mice (white) and *Il-7r*$^{Cre/+}$ *Rbpj*$^{fl/fl}$ mice (black). Data are means ± SEM of three independent

experiments, with two mice of each genotype analyzed per experiment. $^{*}P < 0.05$, $^{**}P < 0.01$, $^{***}P < 0.001$ by Mann Whitney test.

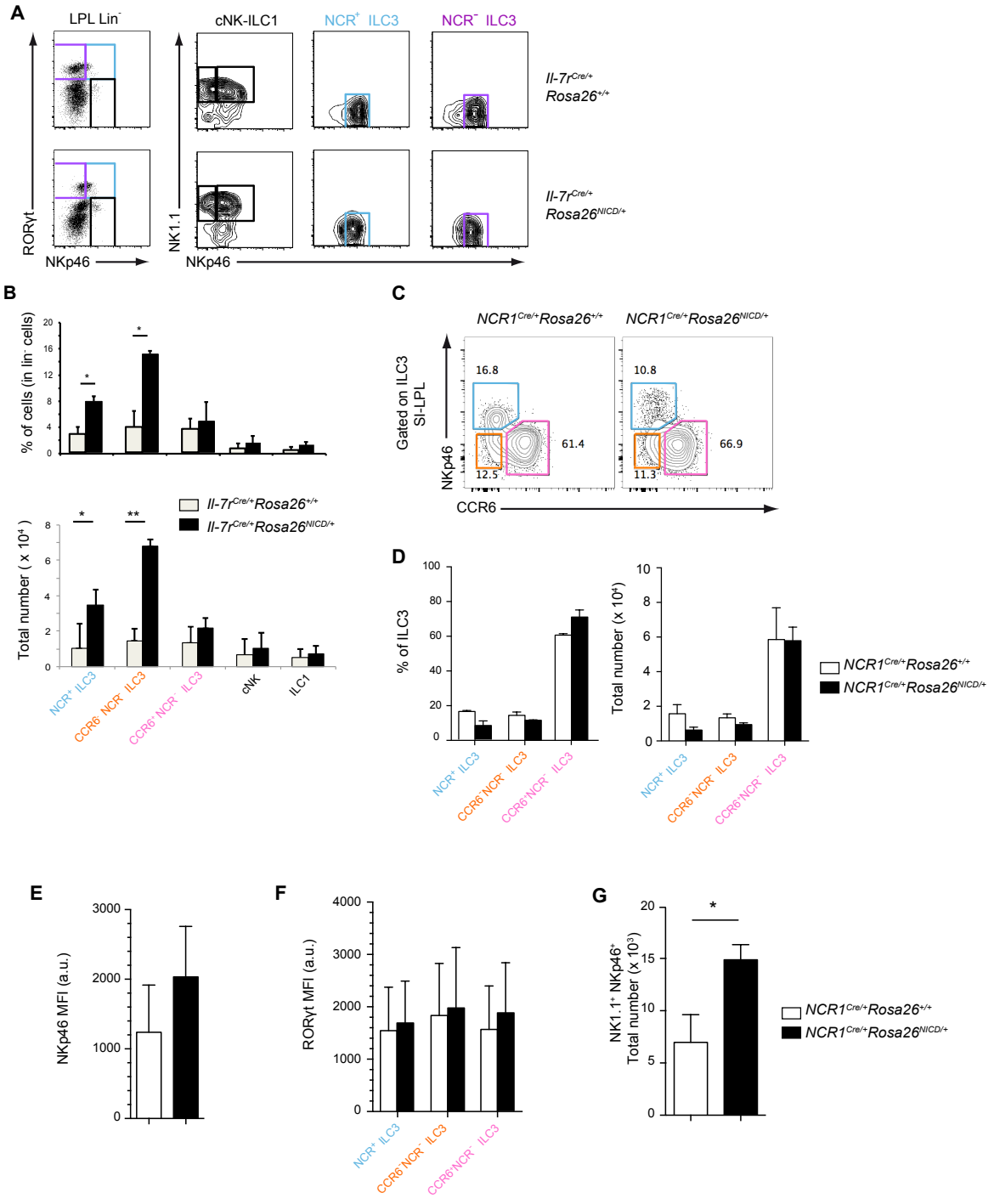
A
LPL Lin-
cNK-ILC1
NCR+ ILC3
NCR- ILC3
Il-7rCre/+ Rosa26+/+
Il-7rCre/+ Rosa26NICD/+
RORγt
NKp46
NK1.1
NKp46
B
% of cells (in lin- cells)
Total number (x 10⁴)
Il-7rCre/+Rosa26+/+
Il-7rCre/+Rosa26NICD/+
NCR+ ILC3
CCR6- NCR- ILC3
CCR6+ NCR- ILC3
cNK
ILC1
C
NCR1Cre/+Rosa26+/+
NCR1Cre/+Rosa26NICD/+
Gated on ILC3 SI-LPL
NKp46
CCR6
16.8
61.4
12.5
10.8
66.9
11.3
D
% of ILC3
Total number (x 10⁴)
NCR1Cre/+Rosa26+/+
NCR1Cre/+Rosa26NICD/+
NCR+ ILC3
CCR6- NCR- ILC3
CCR6+ NCR- ILC3
E
NKp46 MFI (a.u.)
F
RORγt MFI (a.u.)
G
NK1.1+ NKp46+ Total number (x 10³)
NCR1Cre/+Rosa26+/+
NCR1Cre/+Rosa26NICD/+

Fig. 5. Notch signaling favors the differentiation of ILC3s from lamina propria ILC precursors. (**A**) Flow cytometric analysis of cNK-ILC1s, NCR^+ ILC3s, and NCR^- ILC3s in the lamina propria of *Il-7r*$^{Cre/+}$*Rosa26*$^{+/+}$ and *Il-7r*$^{Cre/+}$*Rosa26*$^{NICD/+}$ mice. Data are representative of three independent experiments. (**B**) Percentages (top) and total numbers (bottom) of cNK cells, ILC1s, NCR^+ ILC3s, and NCR^- ILC3s in the lamina propria of *Il-7r*$^{Cre/+}$*Rosa26*$^{+/+}$ mice (white) and *Il-7r*$^{Cre/+}$*Rosa26*$^{NICD/+}$ mice (black). Data are means ± SEM of three independent experiments, with three mice of each genotype analyzed per experiment. (**C**) Flow cytometric analysis of the indicated ILC3 subsets assigned according to their cell-surface expression of NKp46 and CCR6: NCR^+ ILC3s ($NKp46^+CCR6^-$; blue), $CCR6^-$ NCR^- ILC3s ($NKp46^-CCR6^-$; orange), and $CCR6^+$ NCR^- ILC3s ($NKp46^-CCR6^+$; pink). Data are representative of two independent experiments. (**D**) Percentages (left) and total numbers (right) of the indicated ILC3 subsets from *Ncr1*$^{Cre/+}$ *Rosa26*$^{+/+}$ mice (white) and *Ncr1*$^{Cre/+}$ *Rosa26*$^{NICD/+}$ mice (black). (**E**) NKp46 MFIs of NCR^+ ILC3s from *Ncr1*$^{Cre/+}$*Rosa26*$^{+/+}$ mice (white) and *Ncr1*$^{Cre/+}$*Rosa26*$^{NICD/+}$ mice (black). (**F**) RORγt MFIs of the indicated ILC3 subsets from *Ncr1*$^{Cre/+}$*Rosa26*$^{+/+}$ mice (white) and *Ncr1*$^{Cre/+}$*Rosa26*$^{NICD/+}$ mice (black). (**G**) Total numbers of cNK-ILC1s ($NK1.1^+NKp46^+$) from *Ncr1*$^{Cre/+}$ *Rosa26*$^{+/+}$ mice (white) and *Ncr1*$^{Cre/+}$ *Rosa26*$^{NICD/+}$ mice (black). Data in (D) to (G) are means ± SEM of two independent experiments, with two mice of each genotype analyzed per experiment. $^*P < 0.05$, $^{**}P < 0.01$, $^{***}P < 0.001$ by Mann Whitney test.

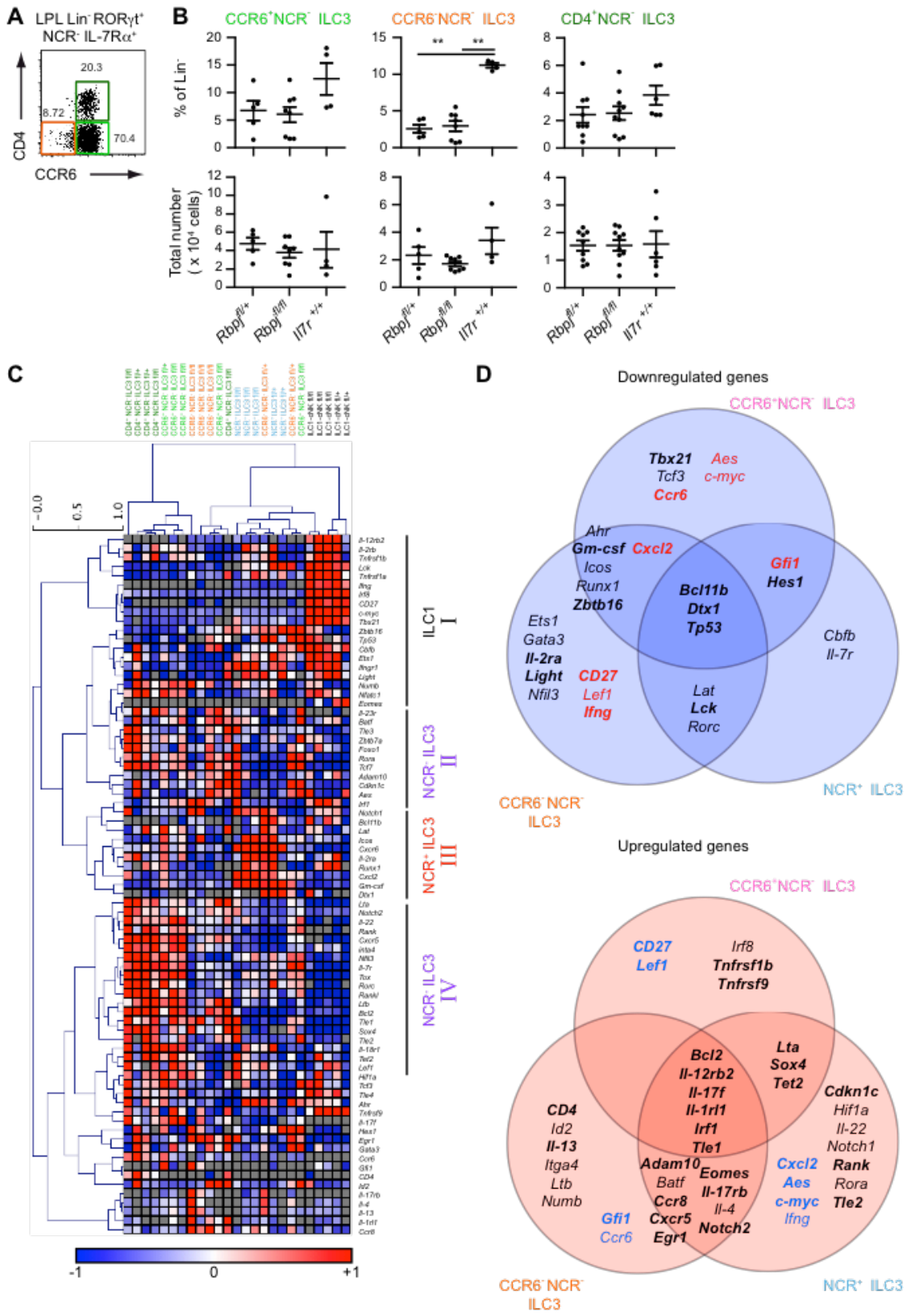
A
LPL Lin⁻ RORγt⁺
NCR⁻ IL-7Rα⁺
20.3
8.72
70.4
CD4
CCR6
B
CCR6⁺NCR⁻ ILC3
CCR6⁻NCR⁻ ILC3
CD4⁺NCR⁻ ILC3
% of Lin⁻
Total number
(x 10³ cells)
**
**
Rbpj fl/+
Rbpj fl/fl
Il7r +/+
C
-0.0
0.5
1.0
ILC1
I
NCR⁻ ILC3
II
NCR⁺ ILC3
III
NCR⁻ ILC3
IV
-1
0
+1
D
Downregulated genes
CCR6⁺NCR⁻ ILC3
Tbx21
Aes
Tcf3
c-myc
Ccr6
Ahr
Gm-csf
Cxcl2
Icos
Runx1
Zbtb16
Gfi1
Hes1
Bcl11b
Dtx1
Tp53
Ets1
Gata3
Il-2ra
Light
Nfil3
CD27
Lef1
Ifng
Cbfb
Il-7r
Lat
Lck
Rorc
CCR6⁻NCR⁻
ILC3
NCR⁺ ILC3
Upregulated genes
CCR6⁺NCR⁻ ILC3
CD27
Lef1
Irf8
Tnfrsf1b
Tnfrsf9
Bcl2
Il-12rb2
Il-17f
Il-1rl1
Irf1
Tle1
Lta
Sox4
Tet2
CD4
Id2
Il-13
Itga4
Ltb
Numb
Adam10
Batf
Ccr8
Cxcr5
Egr1
Eomes
Il-17rb
Il-4
Notch2
Cdkn1c
Hif1a
Il-22
Notch1
Rank
Rora
Tle2
Cxcl2
Aes
c-myc
Ifng
Gfi1
Ccr6
CCR6⁻NCR⁻
ILC3
NCR⁺ ILC3

Fig. 6. The decrease in the number of NCR$^+$ ILC3s in Notch signaling–deficient mice results from loss of the Notch-dependent RORγt$^+$ subset. (**A**) Flow cytometric analysis of NCR$^-$ ILC3 subsets from *Il-7r*$^{+/+}$*Rbpj*$^{fl/+}$ mice. All CD4$^+$NCR$^-$ ILC3s are CCR6$^+$ (dark green), whereas CD4$^-$NCR$^-$ ILC3s are either CCR6$^+$ (light green) or CCR6$^-$ (orange). (**B**) Percentages (top) and total numbers (bottom) of the indicated NCR$^-$ ILC3 subsets from *Il-7r*$^{Cre/+}$*Rbpj*$^{fl/+}$ mice, *Il-7r*$^{Cre/+}$*Rbpj*$^{fl/fl}$ mice, and *Il-7r*$^{+/+}$*Rbpj*$^{fl/+}$ mice. Each data point represents an individual mouse. Data are means ± SEM of at least 3 independent experiments, with 2 mice of each genotype analyzed per experiment. $^*P < 0.05$, $^{**}P < 0.01$, $^{***}P < 0.001$ by Mann Whitney test. (**C**) Single cell multiplex mRNA abundances of cNK-ILC1s, NCR$^+$ ILC3s, and NCR$^-$ ILC3s in the lamina propria of *Il-7r*$^{Cre/+}$*Rbpj*$^{fl/+}$ mice and *Il-7r*$^{Cre/+}$*Rbpj*$^{fl/fl}$ mice. Results are presented as relative to the average expression of housekeeping genes. After hierarchical clustering, data were median-centered and scaled for visualization (red: high expression, blue: low expression, gray: no expression). (**D**) Venn diagrams of the genes that were decreased in expression (top) and the genes that were increased in expression (bottom) in the indicated subsets of cells isolated from *Il-7r*$^{Cre/+}$*Rbpj*$^{fl/fl}$ mice compared to those in the same subsets isolated from *Il-7r*$^{Cre/+}$*Rbpj*$^{fl/+}$ mice. Genes with at least a 1.5-fold change in expression are listed, whereas those with at least a two-fold change in expression are in bold. Genes that are in colors are either increased or decreased in expression in other cell populations. Data are representative of at least two independent experiments, with four mice of each genotype analyzed per experiment. *P* values from statistical analysis of the data in (D) are summarized in table S1.

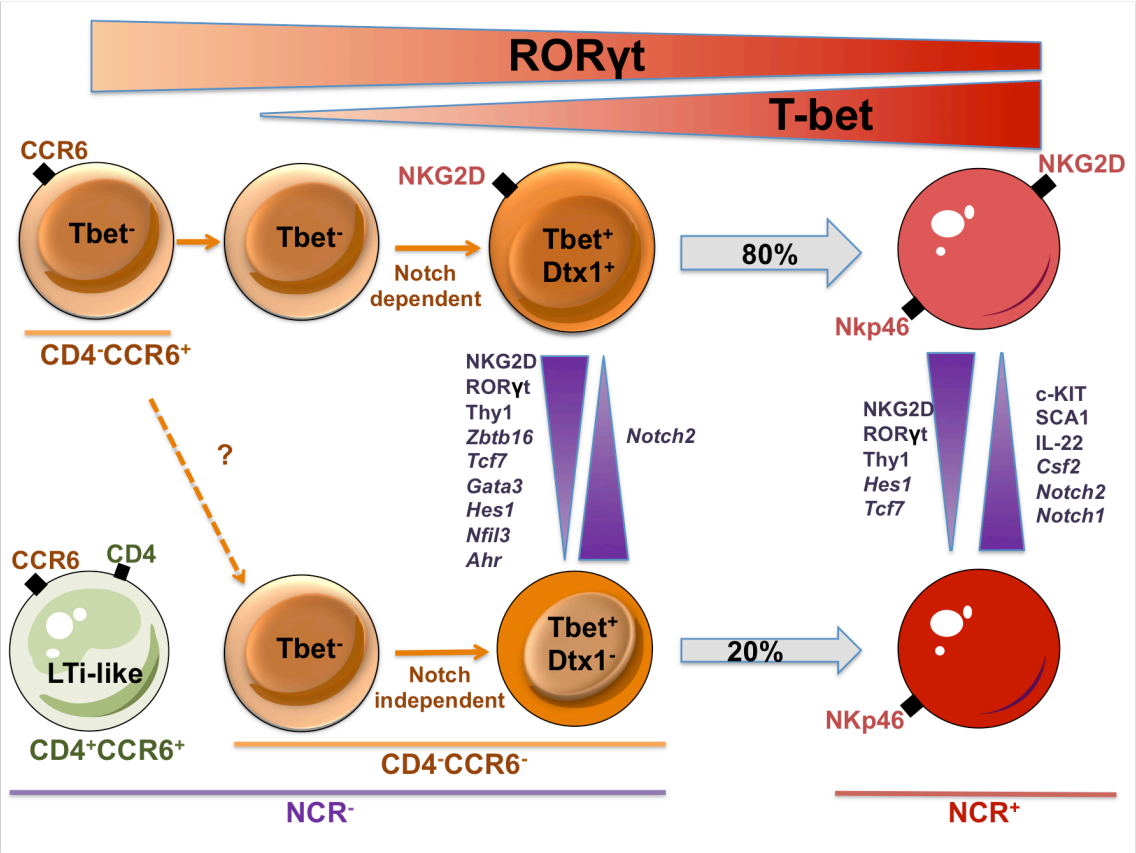
RORγt
T-bet
CCR6
Tbet-
Tbet-
NKG2D
Tbet+
Dtx1+
Notch
dependent
80%
NKG2D
Nkp46
CD4-CCR6+
?
NKG2D
RORγt
Thy1
Zbtb16
Tcf7
Gata3
Hes1
Nfil3
Ahr
Notch2
NKG2D
RORγt
Thy1
Hes1
Tcf7
c-KIT
SCA1
IL-22
Csf2
Notch2
Notch1
CCR6
CD4
LTi-like
Tbet-
Notch
independent
Tbet+
Dtx1-
20%
NKp46
CD4+CCR6+
CD4-CCR6-
NCR-
NCR+

Fig. 7. Schematic representation of the differentiation of intestinal NCR$^+$ ILC3s. The recapitulative model shows that whereas 80% of the NCR$^+$ cells were derived from *Dtx1*$^+$ T-bet$^+$ precursors, the Notch-independent pool was derived from a *Dtx1*$^-$ T-bet$^+$ precursor and represents 20% of the total number of NCR$^+$ cells. The absence of Notch signaling is associated with decreased amounts of NKG2D, RORγt, and Thy1, as well as of transcription factors, such as Zbtb16, Tcf7, Gata3, Hes1, Nfil3 and AhR. Whereas the genes encoding most of these factors are Notch targets, the factors were decreased in abundance, but were not absent, in Notch-independent precursors. Similar to their NCR$^-$ precursors, the Notch-independent NCR$^+$ cells showed decreased amounts of similar proteins (including NKG2D, RORγt, and Thy1) and transcription factors (including Tcf7 and Hes1). They also exhibited specific increases in cKit and Sca1 abundance. The transcripts for *Notch1* and *Notch2* were also both increased in abundance in Notch independent NCR$^+$ cells. The Notch-independent NCR$^+$ cells expressed more *Csf2* transcripts under steady-state conditions and secreted more IL-22 before and after activation than did Notch dependent NCR$^+$ cells. The CCR6$^+$ subset was added to the scheme as an early progenitor of Notch-dependent NCR$^+$ cells because a previous study showed that CD4$^-$ CCR6$^+$ ILC3s can differentiate into NCR$^+$ ILC3s in a T-bet–dependent manner after culture in the presence of Notch ligands (that is, on OP9-Dl1 cells) (*13*).